EC
Journals.ASM.org

Colony Organization in the Green Alga *Botryococcus braunii* (Race B) Is Specified by a Complex Extracellular Matrix

Taylor L. Weiss,[a] Robyn Roth,[b] Carrie Goodson,[c] Stanislav Vitha,[d] Ian Black,[e] Parastoo Azadi,[e] Jannette Rusch,[c] Andreas Holzenburg,[a,d,f] Timothy P. Devarenne,[a] and Ursula Goodenough[c]

Department of Biochemistry and Biophysics, Texas A&M University, College Station, Texas, USA[a]; Department of Cell Biology, Washington University School of Medicine, St. Louis, Missouri, USA[b]; Department of Biology, Washington University, St. Louis, Missouri, USA[c]; Microscopy and Imaging Center, Texas A&M University, College Station, Texas, USA[d]; Complex Carbohydrate Research Center, University of Georgia, Athens, Georgia, USA[e]; and Department of Biology, Texas A&M University, College Station, Texas, USA[f]

***Botryococcus braunii* is a colonial green alga whose cells associate via a complex extracellular matrix (ECM) and produce prodigious amounts of liquid hydrocarbons that can be readily converted into conventional combustion engine fuels. We used quick-freeze deep-etch electron microscopy and biochemical/histochemical analysis to elucidate many new features of *B. braunii* cell/colony organization and composition. Intracellular lipid bodies associate with the chloroplast and endoplasmic reticulum (ER) but show no evidence of being secreted. The ER displays striking fenestrations and forms a continuous subcortical system in direct contact with the cell membrane. The ECM has three distinct components. (i) Each cell is surrounded by a fibrous β-1, 4- and/or β-1, 3-glucan-containing cell wall. (ii) The intracolonial ECM space is filled with a cross-linked hydrocarbon network permeated with liquid hydrocarbons. (iii) Colonies are enclosed in a retaining wall festooned with a fibrillar sheath dominated by arabinose-galactose polysaccharides, which sequesters ECM liquid hydrocarbons. Each cell apex associates with the retaining wall and contributes to its synthesis. Retaining-wall domains also form "drapes" between cells, with some folding in on themselves and penetrating the hydrocarbon interior of a mother colony, partitioning it into daughter colonies. We propose that retaining-wall components are synthesized in the apical Golgi apparatus, delivered to apical ER fenestrations, and assembled on the surfaces of apical cell walls, where a proteinaceous granular layer apparently participates in fibril morphogenesis. We further propose that hydrocarbons are produced by the nonapical ER, directly delivered to the contiguous cell membrane, and pass across the nonapical cell wall into the hydrocarbon-based ECM.**

The trebouxiophyte green fresh- to brackish-water alga *Botryococcus braunii* has a unique colonial organization: individual cells of the colony are embedded in an extracellular matrix (ECM) composed of polymerized and liquid hydrocarbons (LH) (29, 35, 46–48). Although they may serve additional functions, these hydrocarbons notably allow *B. braunii* colonies to float, presumably to increase exposure to light for photosynthesis at the surfaces of ponds or lakes (4). The presence of *B. braunii* oils and ECM fossils in petroleum, coal deposits, and oil shale suggests that their hydrocarbon products once contributed to these reserves (1, 2, 8, 10, 16, 17, 34, 36, 52, 62, 63, 69, 70) and that these hydrocarbons could be used as a source of renewable energy. In fact, *B. braunii* hydrocarbons can be readily converted into petroleum equivalent, drop-in transportation fuels by conventional petroleum-processing techniques (22, 28).

The three races of *B. braunii* are classified on the basis of the chemical nature of the liquid hydrocarbons they produce. The A race primarily produces alkadienes and alkatrienes derived from fatty acids (38, 49, 65, 67); the B race (the focus of this study) produces two triterpenoids, tetramethylsqualene as a minor component, and botryococcenes ranging from C_{30} to C_{37} as the major components (41–43); and the L race produces a tetraterpenoid known as lycopadiene (37, 39). The B race of *B. braunii* has garnered the most research attention due to its ability to accumulate botryococcenes up to 86% of its dry weight (9).

The solid, polymerized-hydrocarbon portion of the ECM of all three races has been found to be mainly composed of long-chain polyacetal hydrocarbons that are covalently, and possibly even noncovalently (mechanically), cross-linked with hydrocarbons specific for each race (47, 48). For example, in the A race, the individual polyacetals appear to be only covalently cross-linked to each other (46). However, the B race further covalently cross-links tetramethylsqualene diols to the polyacetals (48), while the L race further covalently cross-links lycopadiene diols to the polyacetals (6). The B and L races additionally link the tetramethylsqualene and lycopadiene diols to large (C_{31} and C_{33}) macrocyclic aldehydes, which may then be mechanically linked to the linear polyacetals (47). These cross-linked hydrocarbons are proposed to produce a network for deposition of liquid hydrocarbons (47).

An important goal of *B. braunii* research is to develop a comprehensive understanding of how and where the hydrocarbons are produced and retained within the colony. Past research has utilized radioactive precursors to show that in the B race, C_{30} botryococcene is produced inside cells and higher-molecular-weight botryococcenes, C_{31} to C_{34}, are produced by methylation of C_{30} botryococcene with *S*-adenosylmethionine as the methyl donor (43, 74). These studies also indicate that the methylation reactions can take place both inside cells and in the ECM and that intracel-

Received 6 July 2012 **Accepted** 28 August 2012
Published ahead of print 31 August 2012
Address correspondence to Timothy P. Devarenne, tpd8@tamu.edu, or Ursula Goodenough, goodenough@wustl.edu.
Supplemental material for this article may be found at http://ec.asm.org/.

doi:10.1128/EC.00184-12

lular botryococcenes can be transported to the ECM (43), but the mechanism(s) by which this occurs remains unknown. Most current research on *B. braunii* hydrocarbons is focused on identifying the genes responsible for botryococcene biosynthesis, and genes involved in the production of C_{30}, C_{31}, and C_{32} botryococcenes have been identified (54, 55). The enzyme activity associated with C_{30} botryococcene production, and presumably these enzymes, has been shown to be membrane localized (58), likely to the endoplasmic reticulum (ER).

Light microscopy with the fluorescent lipophilic dye Nile red, coupled with confocal Raman microspectroscopy, has documented the presence of botryococcenes in the ECM and in multiple cytoplasmic lipid bodies (LBs) (71), supporting the hypothesis that the lipid-body botryococcenes are secreted out of the cells to form the liquid hydrocarbon portion of the ECM (45, 47). However, direct evidence for this hypothesis has not been obtained.

At the electron microscopy level, several studies have probed the ultrastructure of *B. braunii* cells and colonies, documenting the presence of a wall around each cell (5, 11, 31, 56, 73) and an outer wall surrounding each colony (73). Fibrils of polysaccharide have also been seen emanating from the apexes of individual cells (5, 31, 73). These studies were performed on several different strains of *B. braunii*, and several were carried out before the classification of *B. braunii* into its three races; hence, it is difficult to extend the findings to any specific race. Additionally, the images are compromised by the fact that *B. braunii*, like many other algae with highly impermeable cell walls (CW), is difficult to fix, dehydrate, and embed in plastic (5); moreover, such procedures have the capacity to modify the native organization of extracellular products.

We have therefore analyzed the ultrastructure of the *B. braunii* B race using the quick-freeze deep-etch (QFDE) electron microscopy technique, which employs no fixation or dehydration (20). Living colonies were snap-frozen at liquid helium temperatures (approximately −269°C), fractured at liquid nitrogen temperatures (approximately −196°C), and etched and replicated using platinum/carbon rotary shadowing. In parallel studies, *B. braunii* cells and colonies were subjected to histochemical analysis, while preparations of released outer-wall fragments were subjected to mass spectrometry analysis.

Our findings, many of which are diagrammed in Fig. 1, include the following. (i) An outer retaining wall (RW) serves to sequester the liquid ECM within the colony by forming a drape between cells. A fibrillar sheath extends from the outer face of the retaining wall into the growth medium. A purified preparation of discarded retaining walls/sheath fibrils is ~97% carbohydrate, with 81% of the mass being arabinose (42%) and galactose (39%), the principal sugars of many matrix elements in algae and land plants (30). (ii) The retaining wall also makes intimate contact with the apical cell wall of each cell. A prominent Golgi body and a unique system of fenestrated cortical ER appear to participate in the production and secretion of the retaining wall and its sheath fibrils in this apical domain. Notably, an amorphous secretion product ("toothpaste") is converted into fibrils in conjunction with a proteinaceous granular layer. (iii) The drape also occasionally folds on itself and penetrates the colony's hydrocarbon interior to subdivide a mother colony into daughter colonies, a specialization we term the zipper. (iv) The cell wall, but not the retaining wall, stains intensely with the anionic dye Congo red, indicating that the two walls are composed of distinctive materials and that the cell wall

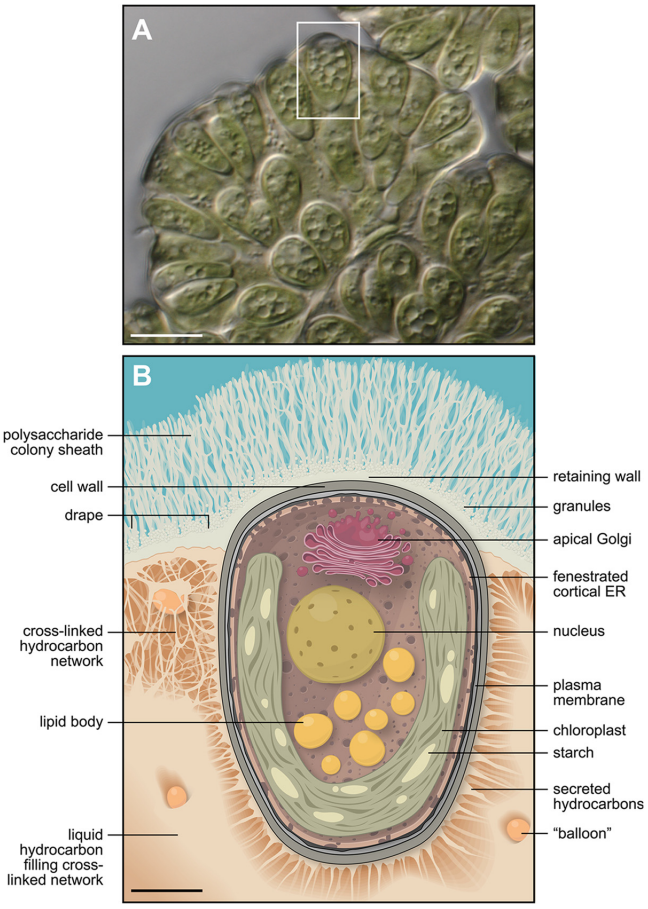

FIG 1 Model of a *B. braunii* cell within a colony based on the studies presented here. (A) Color DIC microscopy image of a partial *B. braunii* colony. The boxed area is depicted in panel B. Bar, 10 μm. (B) Model of the *B. braunii* cell and its surrounding extracellular matrices. Portions of the hydrocarbon ECM around the cell edge and the upper left quadrant are drawn with the liquid hydrocarbons removed to show the underlying structure of these regions. For simplification, not all cellular organelles are shown. Bar, 2 μm.

contains β-1,4- and/or β-1,3-glucans. (v) The cytoplasmic interior contains inclusions, corresponding to those visualized with Nile red and confocal Raman microspectroscopy, that are visually indistinguishable from triacylglycerol (TAG)-containing lipid bodies in other algae. No evidence of their secretion was encountered. (vi) In the nonapical portions of the cell, a fenestrated ER is in intimate contact with the cell membrane. We propose that botyrococcenes produced by this ER are directly delivered to the cell membrane, after which they are exuded across the cell wall and into the ECM. (vii) The hydrocarbon ECM fills the interstices between cells. The botryococcene liquid hydrocarbon phase is deformable to fracture and largely extracted by *n*-hexane, while the polymerized phase is fibrous and not extracted by *n*-hexane. We propose that the polymerized polyacetals function to stabilize the colony and to facilitate gas exchange in the colony interior.

MATERIALS AND METHODS

Strains and culture conditions. *B. braunii* strain Berkeley (Showa) race B (57) was grown in modified Chu 13 medium (19) using 13-W compact fluorescent 65 K lighting at a distance of 7.62 cm, which produced a light intensity of 280 μmol photons/m^2/s. Lighting was on a cycle of 12-h

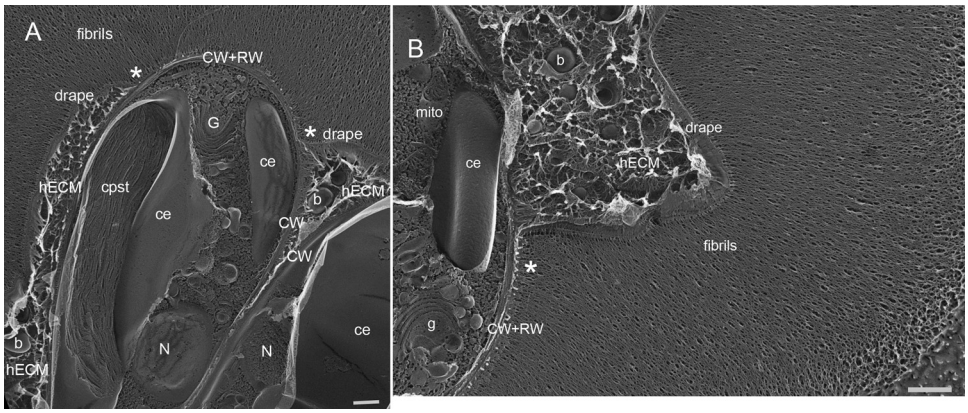

FIG 2 Survey views of *B. braunii* colony organization. (A) Two cells showing nucleus (N), chloroplast (cpst), chloroplast envelope (ce), and apical Golgi body (G). The intercellular space is filled with an h-ECM containing balloons (b). The retaining wall and cell wall cover the apex of the cell at left, and the retaining wall extends between cells to form a drape that holds in the h-ECM. The asterisks indicate the cell apex-drape junctions. Sheath fibrils extend from the retaining wall. Bar, 500 nm. (B) Cell with apical Golgi body (g), retaining wall carrying white tubular elements, cell wall, and mitochondria (mito). The drape retaining wall holds in the h-ECM with balloons (b), with an asterisk at the cell-drape junction. The full extent of the fibrillar sheath is depicted (bottom right). Bar, 500 nm.

light/12-h dark at 22.5°C. The cultures were continuously aerated with filter-sterilized enriched air containing 2.5% CO_2. Fifty milliliters of culture was used to inoculate 750 ml of subsequent subcultures every 4 weeks.

Quick-freeze deep-etch electron microscopy. Floating colonies were pipetted from the surfaces of fresh cultures, placed on a cushioning material, and dropped onto a liquid He-cooled copper block; the frozen material was transferred to liquid nitrogen and fractured, etched at −80°C for 2 min, and Pt/C rotary replicated as described previously (20). The replicas were examined with a JEOL electron microscope, model JEM 1400, equipped with an AMTV601 digital camera. The images are photographic negatives; hence, protuberant elements of the fractured/etched surface are most heavily coated with platinum and appear white.

Histochemical staining and microscopy. For visualization of the cell wall using Congo red (Sigma), 100 μl of *B. braunii* colonies in medium was treated with 1 μl of a 1-mg/ml stock solution of Congo red dissolved in water. For visualization of botryococcenes and other lipids using Nile red (Sigma), 400 μl of *B. braunii* colonies in medium were treated with 1 μl of a stock solution of Nile red dissolved in acetone (0.15 mg/ml) so that the final concentrations of Nile red and acetone were 0.375 μg/ml and 0.25%, respectively. Both Congo red- and Nile red-stained samples were kept in the dark and incubated at room temperature for 15 min. Both samples were then diluted with 1 ml distilled water (dH_2O) and centrifuged at 10,000 × *g* for 30 s, and excess solution was removed by pipetting under the floating layer of algal colonies. This rinsing process was quickly repeated three times, and the final stained algal samples were stored in a minimal volume prior to immediate microscopy.

The fibril sheath system was visualized using a modified periodic acid-Schiff reagent (mPAS) using propidium iodide (PI) (Sigma) as the Schiff reagent (53). *B. braunii* colonies (270 μl) in medium were treated with 30 μl of a stock solution of 10% periodic acid in the dark at room temperature for at least 30 min. The samples were diluted with 1 ml dH_2O and centrifuged at 10,000 × *g* for 30 s, and excess solution was removed by pipetting under the floating layer of algal colonies. This rinsing process was repeated three times. The samples were then resuspended in 30 μl of 10 mM PBS buffer, pH 8.0, and 1 μl of a 1-mg/ml PI stock solution was added. The samples were kept in the dark and incubated at room temperature for 20 min before an additional rinse with dH_2O (three times) and immediate microscopy visualization. Costaining of *B. braunii* colonies with both Nile red and an mPAS reaction followed the same procedure as an mPAS reaction alone, except that 1 μl of Nile red stock solution was added to the sample during the PI incubation.

Microscopy imaging of *B. braunii* colonies was performed at the Texas A&M University Microscopy and Imaging Center. Fluorescence microscopy visualization was performed using an Olympus FV1000 (Olympus America Inc., Center Valley, PA) laser scanning confocal microscope equipped with an UPLSAPO 100×/1.4 oil immersion objective. Excitation and emission wavelengths were set for Congo red (excitation, 543 nm; emission, 555 to 630 nm), mPAS with PI (excitation, 543 nm; emission, 555 to 620 nm), Nile red (excitation, 488 nm; emission, 540 to 590 nm), and Nile Red plus mPAS with PI double staining (excitation, 488 nm; emission, 500 to 550 and 620 to 640 nm, sequential acquisition). Chlorophyll autofluorescence (excitation, 405 nm; emission, >650 nm) was recorded in parallel with the dyes listed above, using line-sequential acquisition.

Shell preparation. Five liters of a 4-week-old *B. braunii* culture was left undisturbed for 12 h, allowing a majority of colonies to float and residual material to settle. This residual material was then harvested by vacuum suction with care to minimize disruption of the floating algal layer. The harvested material was vacuum filtered through a 35-μm nylon cloth (Aquatic Eco-Systems, Inc., Apopka, FL) to remove residual large algal colonies. The filtrate was centrifuged at 17,000 × *g* for 30 min to pellet the shells, bacteria, and any remaining algal colonies in solution. The supernatant was carefully disposed of by vacuum suction, and the soft layer of shells was gently resuspended and transferred into fresh centrifugation tubes, leaving behind a hard pellet of bacteria and algal colonies. The resuspended shells were diluted with dH_2O, centrifuged at 48,000 × *g* for 15 min, and again harvested. This process of centrifugation, shell isolation, and dH_2O rinsing was repeated at least 4 times until there was no obvious pellet of bacteria after centrifugation. The shell fraction was then freeze-dried and analyzed by mass spectrometry as described below.

Carbohydrate mass spectrometry analysis. For glycosyl composition, the shell preparation was analyzed by the per-*O*-trimethylsilyl (TMS) and alditol acetate derivatization methods. For the TMS method, methyl glycosides were prepared from the dry sample by methanolysis in 1 M HCl in methanol at 80°C for 17 h, followed by re-*N*-acetylation with pyridine and acetic anhydride in methanol (for detection of amino sugars). The sample was then per-*O*-trimethylsilylated by treatment with Tri-Sil (Pierce) at 80°C for 0.5 h. The TMS derivatives were run on a Shimadzu QP2010 gas chromatograph-mass spectrometer (GC-MS) in chemical ionization mode. For the alditol acetate method, the sample was depolymerized, reduced, and acetylated; the resultant alditol acetates (AAs) were analyzed by GC-MS for determination of monosaccharide identity. Specifically, 200 μg of lyophilized shells was hydrolyzed using 2 M trifluoroacetic acid for 2 h in a sealed tube at 121°C, reduced with sodium tetradeuteroborate ($NaBD_4$), and acetylated using acetic anhy-

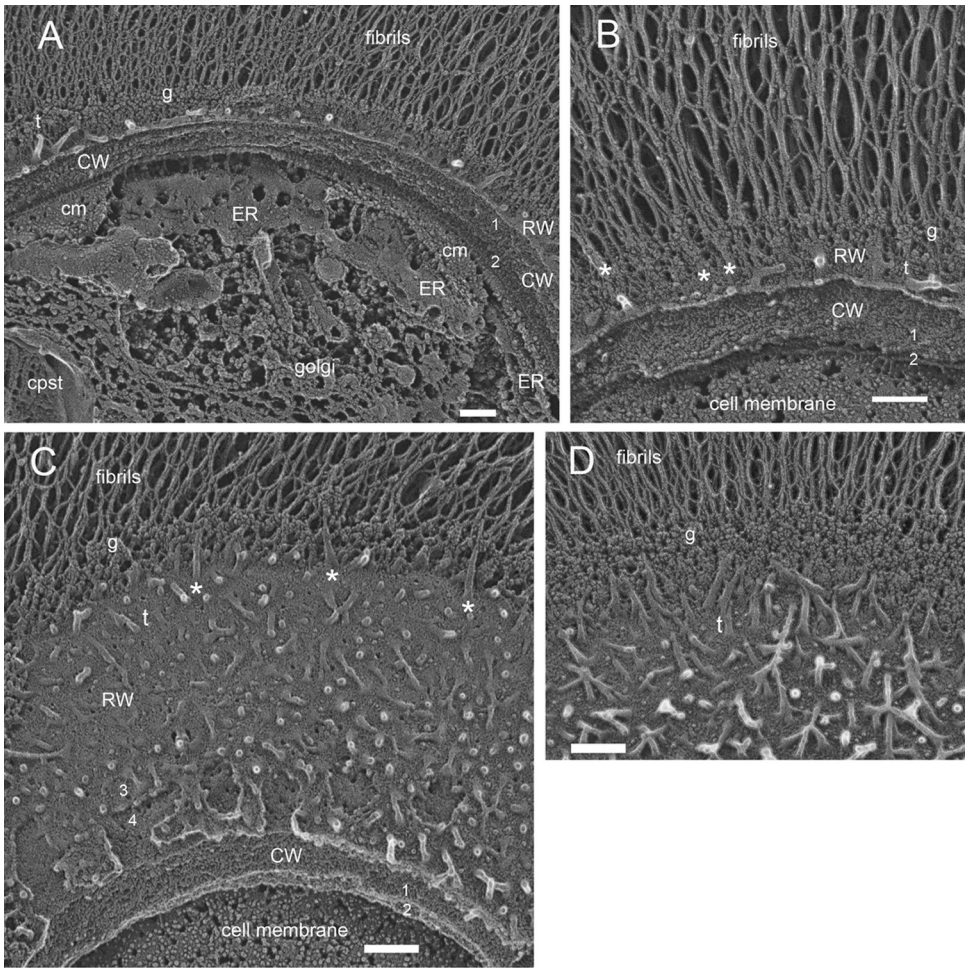

FIG 3 Cell apexes. (A) Apical Golgi body, fenestrated ER, and cell membrane (cm) underlie the cell wall, which fractures into 2 layers (labeled 1 and 2) at right, and retaining wall. The retaining wall carries white tubules (t), a layer of granules (g), and the fibrillar sheath. cpst, chloroplast. Bar, 100 nm. (B) Cell membrane, double-layered (labeled 1 and 2) fibrous cell wall, and retaining wall carrying tubules (t), granules (g), and fibrils. The asterisks mark continuities between tubules and fibrils. Bar, 100 nm. (C) Cross-fractured fibrous double-layered (labeled 1 and 2) cell wall overlain by *en face* view of the retaining wall, which fractures into 2 layers (labeled 3 and 4), showing tubules (t) and granules (g). The asterisks mark continuities between tubules and fibrils. Bar, 100 nm. (D) Retaining wall *en face* with tubules (t), granules (g), and fibrils. Bar, 100 nm.

dride/trifluoroacetic acid. The AAs were analyzed on an Agilent 7890A GC interfaced to a 5975 mass selective detector (MSD) operating in the electron impact ionization mode. Separation of the AAs by GC was performed on a 30-m Supelco 2330 bonded-phase fused-silica capillary column.

For glycosyl linkage analysis, the samples were permethylated, depolymerized, reduced, and acetylated, and the resultant partially methylated alditol acetates (PMAAs) were analyzed by GC-MS as previously described (79). Initially, ~1 mg of the sample was suspended in 200 μl of dimethyl sulfoxide, and the sample was left to stir for 3 days. The sample was then permethylated by treatment with sodium hydroxide and methyl iodide in dry dimethyl sulfoxide (DMSO) (12). Following sample workup, the permethylated material was hydrolyzed using 2 M trifluoroacetic acid for 2 h in a sealed tube at 121°C, reduced with $NaBD_4$, and acetylated using acetic anhydride/trifluoroacetic acid. The resulting PMAAs were analyzed on an Agilent 7890A GC/5975 MSD as described above. Separation was performed on a 30-m Supelco 2330 bonded-phase fused-silica capillary column.

Protein determination and SDS-PAGE of lyophilized shells. For protein determination, 1.6 mg of shell lyophilate was suspended in 200 μl water and assayed with the Bio-Rad Bradford Protein Assay reagent using bovine serum albumin (BSA) as a standard. For SDS-PAGE, 22.5 mg of sample was brought up in 100 μl extraction buffer (1 mM NaCl, 10 mM Tris, pH 7, protease inhibitor cocktail), 100 μl 2× Laemmli buffer was added, and the sample was heated at 90°C for 5 min and then applied to a 4 to 15% polyacrylamide gradient gel (Bio-Rad). The gels were stained with Coomassie blue.

Shells on coverslips. Coverslip chips (3 by 3 mm) were immersed in 1 mg/ml low-molecular-weight (LMW) polylysine (1,000 to 4,000 MW; Sigma P0879) in 100 mM KCl for 1 h and rinsed in water. Two chips were placed on the bottom of a 1.5-ml microcentrifuge tube containing a polished resin insert that provided a flat base, and 50 μl of a freshwater-washed shell pellet was layered over 400 μl water and spun in a clinical centrifuge (7,300 rpm) for 6 min. The chips were transferred to water, immediately quick frozen, and stored in liquid nitrogen until they were mounted in a Balzers freeze-etch device, where they were immediately warmed to −80°C, freeze-dried for 15 min *in vacuo*, and replicated with platinum/carbon.

***n*-Hexane extraction.** In a modified version of a previously described process (15), colonies were applied to a 35-μm mesh nylon filter sandwiched between 2 trimmed 1-ml pipette tips. Compressed air was passed through the filter for 1 min, the filter was removed, and colonies were

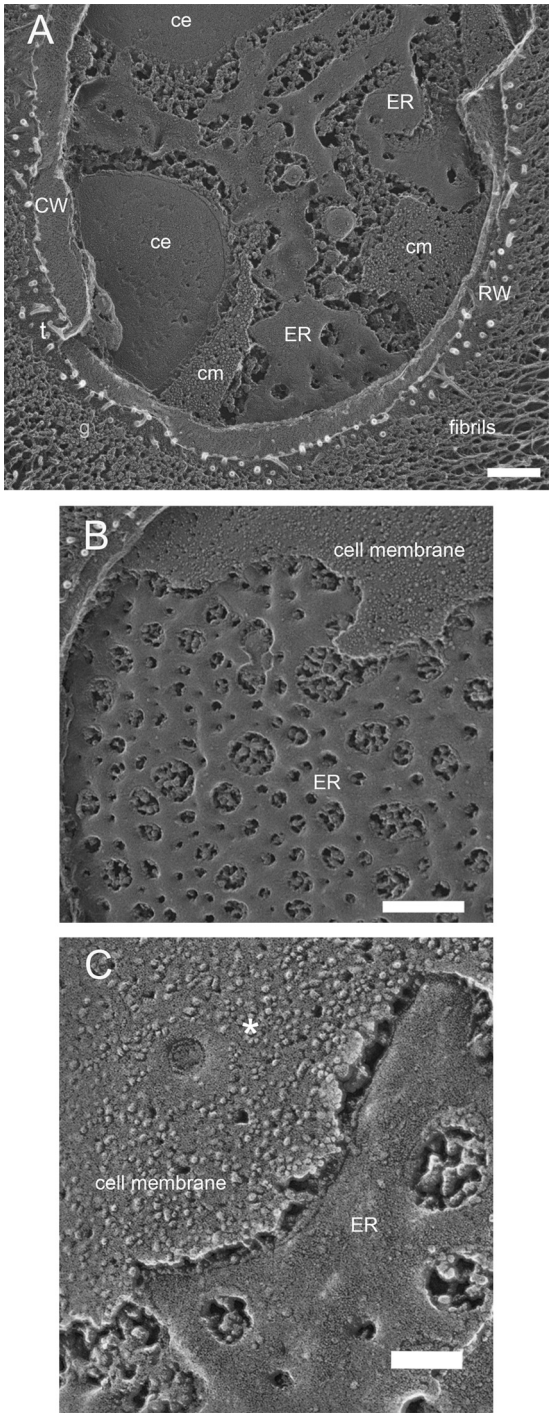

FIG 4 (A and B) Apical fenestrated ER and the overlying cell membrane (cm), cell wall, and retaining wall with its tubules (t), granular layer (g), and fibrils. ce, chloroplast envelope. (C) The asterisk marks a secretion pore in the cell membrane. Bars, 250 nm (A), 200 nm (B), and 100 nm (C).

spread uniformly over its surface and air dried for 10 min. The dried colonies were removed from the filter and placed in a capped glass tube containing 12 ml *n*-hexane (Sigma H9379) and a stir bar, and stirred for 1 h, during which the *n*-hexane turned yellow. The *n*-hexane was removed by aspiration, and the cells were dispersed in 5 ml phosphate-buffered saline (PBS) and washed 2 times before freezing.

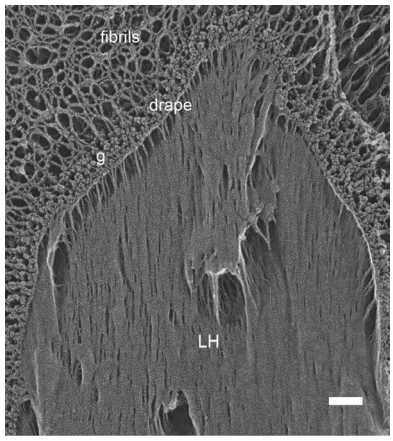

FIG 5 Drape domain of the retaining wall with associated granules (g) and fibrils on its external face and LH on its internal face. Bar, 100 nm.

RESULTS

Overview of colony organization. The organization of a *B. braunii* cell and the surrounding ECM of the colony are diagrammed in Fig. 1. Each colony unit, containing 50 to 100 ovoid cells organized into smaller clusters and embedded in a hydrocarbon extracellular matrix (h-ECM), is encased in a retaining wall. The outer surface of the retaining wall carries an extensive system of anastomosing fibrils that extends 2 to 3 μm into the growth medium and forms a fibrillar sheath around the entire colony; this presumably corresponds to the "tenuous mucilage layer surrounding the colony" described in 1936 (7) and the fibrillar sheath described later (73). The inner surface of the retaining wall has two configurations: (i) when overlying the apical portion of a cell, it makes direct contact with the CW; (ii) when spanning the region between cells, it makes direct contact with the h-ECM and forms a "drape" between the cells.

Figure 2 illustrates these general features in QFDE replicas (additional survey images are found in File S1 in the supplemental material). The asterisks indicate junctions between cell wall-associated and drape domains of the retaining wall. Also evident is the highly heterogeneous nature of the h-ECM, as detailed below.

The retaining wall-cell wall-ER system at the cell apex. Figure 3A illustrates key features of the cell apex in cross-fracture (additional images of the cell apex are found in File S2 in the supplemental material). The thin RW is in direct contact with the thicker fibrous CW, which often fractures into two sublayers (Fig. 3A, labeled 1 and 2; see File S3 in the supplemental material), beneath which is the cell membrane (cm) and then a fenestrated ER cisternum. A large Golgi body also occupies the apical cytoplasm (Fig. 1 and 2; see File S3 in the supplemental material). The outer aspect of the retaining wall carries the fibrillar sheath system plus two additional differentiations: protuberant tubular elements (t), resembling toothpaste, and a layer of granules (g).

Figure 3B to D shows these differentiations in *en face* fractures. The retaining wall, which fractures into two sublayers (Fig. 3C, labeled 3 and 4; see Fig. S2-4 in File S2 and Fig. S3-2 in File S3 in the supplemental material), carries abundant tubular elements that "dive into" the granular material; fibrils emerge from the other side of the granular layer. Asterisks in Fig. 3B and C denote tubules that display direct continuity with branching fibrils. It is therefore

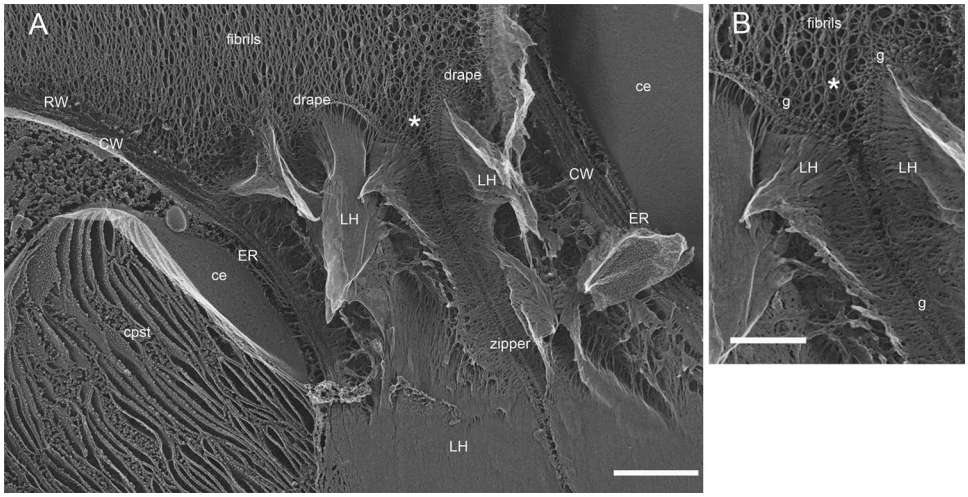

FIG 6 Retaining-wall zipper. (A) Apical domains of two cells embedded in LH and interconnected by a drape. At the asterisk, the drape forms a zipper that extends into the colony interior. RW, retaining wall carrying a few white tubules; cpst, chloroplast; ce, chloroplast envelope. Bar, 500 nm. (B) Higher magnification of zipper involution (asterisk). Fibrils are absent, and granules (g) coalesce as a central domain of the zipper flanked by two RW domains. Bar, 250 nm.

proposed that a tubule-to-fibril transformation occurs at the retaining-wall surface in association with the granules.

Figure 4A to C shows *en face* fractures of the fenestrated ER that directly underlies the apical cell membrane. In Fig. 4A, the fracture plane has dropped below the cell membrane to reveal a segment of the ER; in Fig. 4B, a continuous expanse is exposed. The ER fenestrae are irregular in size; whether this is native or due to differential fracture/etching is not known. At higher magnification (Fig. 4C), the asterisk marks a candidate secretion pore in the cell membrane (additional secretion pore candidates are found in File S4 in the supplemental material). As detailed in Discussion below, these pores are interpreted as arising when polysaccharide material, delivered to the fenestrae via Golgi body-derived vesicles, passes through the cell membrane and then traverses the cell and retaining walls, emerging as the tubules on the external face of the retaining wall.

The retaining-wall system in intercellular drapes. At the junctions marked by asterisks in Fig. 2, the retaining wall loses its association with the apical cell wall and drapes across the h-ECM, eventually making contact with the apical cell walls of adjacent cells. Figure 5 shows such a drape at high magnification (additional images of drapes and h-ECM are found in File S5 in the supplemental material). The granular layer and the fibrils remain associated with the drape, but the tubular elements are absent, indicating that the tubules are a unique feature of the retaining-wall–cell wall relationship.

The h-ECM in Fig. 5 displays two phases: delicate strands associate with the inner aspect of the retaining wall, and amorphous material fills the rest of the region. As detailed below, the amorphous material represents the LH phase of the h-ECM. The strands are possibly polymerized hydrocarbons but are more likely liquid hydrocarbons sheared during the fracturing process.

Retaining-wall "zipper." Figure 6A shows two cells and their intervening drape. At the asterisk, the drape dives into the h-ECM, forming a configuration that we designate a retaining-wall zipper. Figure 6B enlarges the region of zipper initiation. The drape, no longer bearing fibrils, folds in on itself to form a trilaminar unit consisting of a retaining wall, a shared granule domain, and a second retaining wall. Candidate *en face* views of the zipper wall are shown in File S6 in the supplemental material. As detailed in Discussion below, we propose that zippers function to segregate a colony into daughter colonies, with the granule domain possibly serving as the plane of daughter-colony separation.

"Shells," excised segments of the retaining wall. As *B. braunii* cultures grow, uniform cup-shaped structures, ~3 by 5 μm in size, accumulate in the medium (Fig. 7A). These "shells" form a fluffy pellet when the medium is centrifuged (Fig. 7B), and highly purified shell preparations can be obtained with filtering and washing (Fig. 7C). QFDE shows the shells to be segments of the retaining wall and its fibril sheath (Fig. 7D, 8, and 9; additional images are shown in File S7 in the supplemental material). Remarkably, although the culture is not axenic (Fig. 7B), the shells resist degradation for many weeks.

Figure 8 shows representative images of shells snap-frozen in aqueous suspension. The retaining-wall fibrils radiate outward, with the layer of granules at their base (Fig. 8A and B), and the inner face of the retaining wall faces the curved interior, mirroring the topology adopted at the cell apexes. Cross-fractures of the retaining wall (Fig. 8A and B, single asterisks) reveal it to be very narrow (~15 nm); *en face* fractures (Fig. 8A and B, double asterisks) show a smooth surface that, when deeply etched (Fig. 8C), has a roughened texture with no evidence of a fibrous component (see Fig. S7-1 to -3 of File S7 in the supplemental material for additional images); in contrast, the cell wall is thicker (~50 nm) and visibly fibrous (Fig. 3A to C and 4A; see Fig. S3-1 and -2 of File S3 in the supplemental material). Shells lack the tubular toothpaste-like elements; this could indicate that they derive from drape domains, which lack these elements (Fig. 5), or that they derive from apical domains that have lost the tubules during or following the excision process.

Figure 9A and B shows shells adsorbed to a polylysine-coated glass coverslip, revealing the smooth face of the retaining wall and the full dimensions of the fibrillar sheath.

The granular material interfacing the tubules and fibrils of the

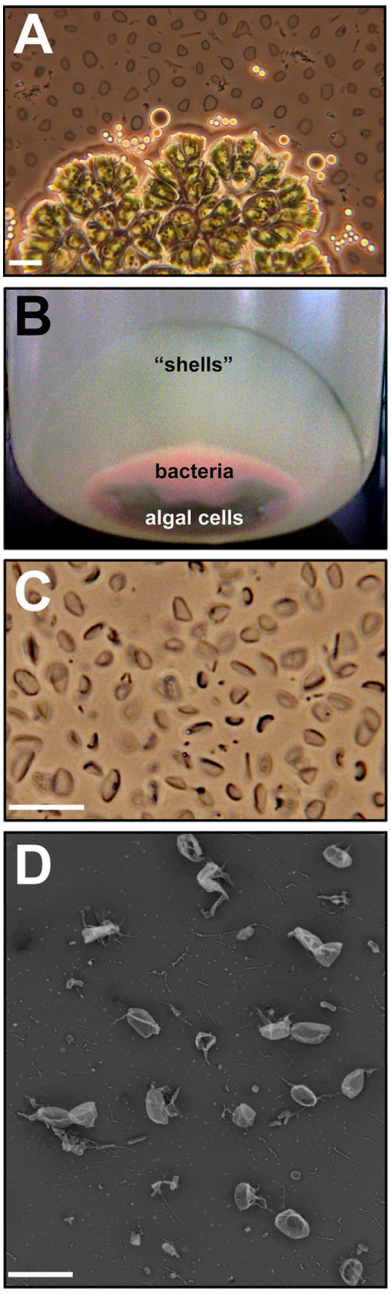

FIG 7 Isolation and imaging of *B. braunii* "shells." (A) Portion of a *B. braunii* colony, induced by pressure on the coverslip to exude h-ECM globules (note that this does not occur spontaneously), with shells in the surrounding medium. Bar, 10 μm. (B) Centrifugation of nylon cloth-filtered *B. braunii* culture medium pellets the shells, along with bacteria and dead algal cells. Shell purification is achieved by repeated harvesting and centrifugation. (C) View of final shell preparation by phase microscopy. Bar, 10 μm. (D) View of freeze-dried shells by QFDE showing their cupped shape and fibrillar endowment. Bar, 10 μm.

retaining wall (Fig. 3 to 5) persists in the shell preparation (Fig. 8A and B). Since the granules resemble proteins, the presence of protein in the shell lyophilate was assayed, and it was estimated to represent 1.25% of the total mass (Table 1). SDS-PAGE of the shell lyophilate documented the presence of a single prominent polypeptide (Fig. 10) with an apparent molecular mass of 150 kDa. We propose that this polypeptide forms the granules.

Histochemical and chemical analysis of cell and retaining walls and the fibril sheath system. Histochemical studies provided additional information about the ECM components of *B. braunii*. Nile red stained the intracellular LBs and the intercellular hydrocarbon matrix (Fig. 11A to D), as expected, and Congo red, which stains β-1,4- and β-1,3-glucans, including cellulose (13, 32, 76), showed strong and specific staining of the cell perimeters (Fig. 11E to I), indicating that the cell wall is composed of a cellulose-like polysaccharide. However, neither reagent stained the retaining wall/sheath (Fig. 11), nor is it visible with color differential interference contrast (DIC) (Fig. 12A), although a haze around the colony edge is visible with black-and-white DIC (Fig. 12B).

Since several previous studies indicated the presence of polysaccharide associated with the colony exterior (5, 31, 73), we next used a more general polysaccharide stain, the periodic acid-Schiff reagent (PAS) stain, in which carbohydrate vicinal diols are oxidized to aldehydes with periodic acid and the aldehydes are then detected with the Schiff reagent (23). We employed an mPAS reaction that utilizes PI as the Schiff reagent (53), and this procedure was capable of effectively staining polysaccharides in the chloroplast (presumably starch), in the cell wall, and in the retaining-wall–fibrillar-sheath system (Fig. 12C to F; see Fig. S8-1 of File S8 in the supplemental material), suggesting that the last is composed of carbohydrates. Costaining with mPAS and Nile red (Fig. 13A to F) revealed the extensive Nile-red-positive h-ECM in which each of the cells was embedded and the mPAS-positive system that surrounds the entire colony and penetrates to define the lobes of future daughter colonies. As detailed in Discussion below, we propose that retaining-wall zippers correspond to the internal mPAS-positive system.

We next subjected the shell preparation, which includes retaining wall/fibrillar sheath and granules (Fig. 8 to 9), to TMS and alditol acetate derivatization followed by GC-MS. The analysis (Table 1) showed that the shells are 97.9% carbohydrate, with the major glycosyl residues being arabinose (46.7 mol%) and galactose (36.3 mol%). Mannose and glucose were trace components. Two unidentified deoxyhexose peaks constituting 9.3 mol% (Table 1) were detected in the sample using the TMS derivatization method, followed by chemical-ionization GC-MS detection. The sample also contained minor amounts of the uncommon glycosyl residues 3-methyl-arabinose and 6-methyl-galactose. Interestingly, the TMS derivatization did not detect any uronic acids or *N*-acetyl glycosyl residues (not shown), indicating that the polysaccharides in the shells do not possess additional chemical modifications commonly associated with structural carbohydrates.

We also analyzed the glycosyl linkages of the polysaccharides in the shell material. As would be expected from the composition analysis, the majority of the linkages involve galactose and arabinose (Table 2). The arabinoses and deoxyhexoses are mainly linked at just one position: the 1 carbon (terminally linked) or the 2 carbon (Table 2). The galactoses mainly have two linkages per single unit, 2,3-linked and 2,4-linked; a small amount is triple linked at the 3, 4, and 6 carbons or singly linked at the 4 carbon (Table 2). All other identified linkages were saccharides with only one linkage (Table 2), suggesting that the polysaccharide chains have a backbone of galactose that terminates with, or has side chains of, only one saccharide, mainly arabinose. Since there are none of the more common 1,4 or 1,6 linkages, this polysaccharide

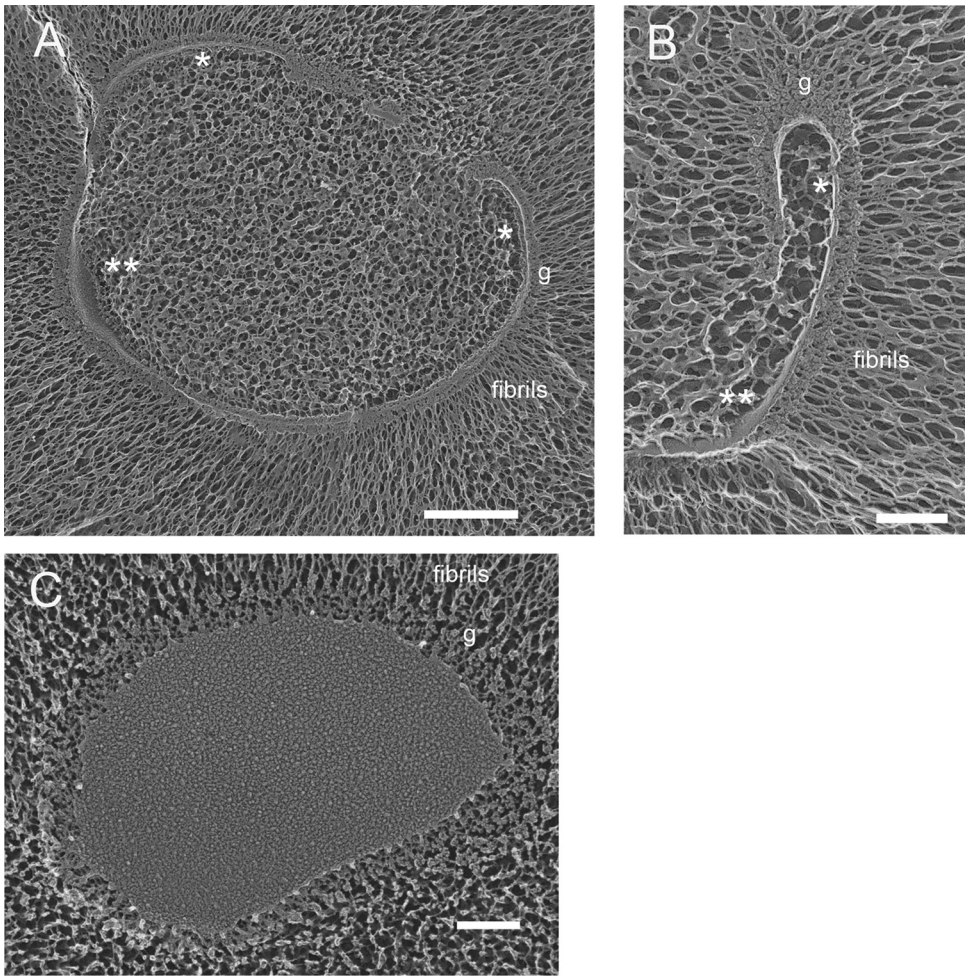

FIG 8 Shells suspended in buffer. (A and B) Retaining walls seen in cross-fracture (asterisk) and *en face* fracture (double asterisks) with overlying granules (g) and sheath fibrils. (C) Deeply etched retaining wall showing granular texture. Bars, 500 nm (A), 200 nm (B), and 500 nm (C).

clearly has an unusual structure; more extensive analyses are ongoing and will be published separately.

The hydrocarbon extracellular matrix: *in situ* and *n*-hexane extracted. The *B. braunii* h-ECM, while highly heterogeneous, displays 3 distinctive morphological domains.

(i) Liquid hydrocarbon botryococcenes. The homogeneous material shown in Fig. 5 is identified as LH, or botryococcenes, based on its morphology and the fact that it is largely removed when the colonies are dried and exposed to *n*-hexane (see below), a procedure that extracts this component of the ECM (38, 42). The inner surfaces of retaining walls and the outer surfaces of cell walls are fully coated with liquid hydrocarbon (Fig. 2 and 14; see File S5 in the supplemental material), except at the cell apexes, where the two walls are instead in contact with one another (Fig. 2 to 4).

The liquid hydrocarbon is visibly deformable to the fracturing process (Fig. 5). Indeed, it is not uncommon to encounter regions, such as those marked with asterisks in Fig. 14B, where the hydrocarbon has "splatted" onto a previously fractured face of a cell.

While the liquid hydrocarbon usually appears compact, as in Fig. 5 and 14A and B, it occasionally forms rivulets (Fig. 14C), underscoring its liquid properties, and it commonly adopts a "spikey" appearance when contiguous to the cell wall (Fig. 14A and B).

(ii) Balloons. Common inclusions in the liquid hydrocarbon phase are round-to-ovoid structures that we designate "balloons" (labeled b in Fig. 2 and 14A and C; see File S5 in the supplemental material). Although the fracture plane usually travels along their outer contours, occasional cross-fractures (Fig. 14D) reveal that the balloons are neither hollow nor solid but rather contain aggregated material. These structures do not stain with Nile red and are easily visible in the ECM of a Nile red-stained colony (see Fig. S8-2 of File S8 in the supplemental material).

(iii) Polymerized hydrocarbon. h-ECM domains also display strands of material (Fig. 2, 5, and 14), but it is difficult to ascertain which of these arise as the consequence of mechanical distortion of the liquid hydrocarbon phase and which represent images of the polymerized and cross-linked hydrocarbons known to occupy the h-ECM (47, 48). To address this question, colonies were dried and treated with *n*-hexane to extract the liquid hydrocarbon phase. In regions where extraction is evidently complete (Fig. 15A), an extensive system of filamentous material is exposed; in regions where extraction is partial (Fig. 15B), filamentous and liquid regions are interspersed. We propose that these filaments represent the *n*-hexane-insoluble polymerized hydrocarbons. Notably, balloons persist in extracted samples (Fig. 15), indicating that they are not targets of *n*-hexane solubilization. Additional

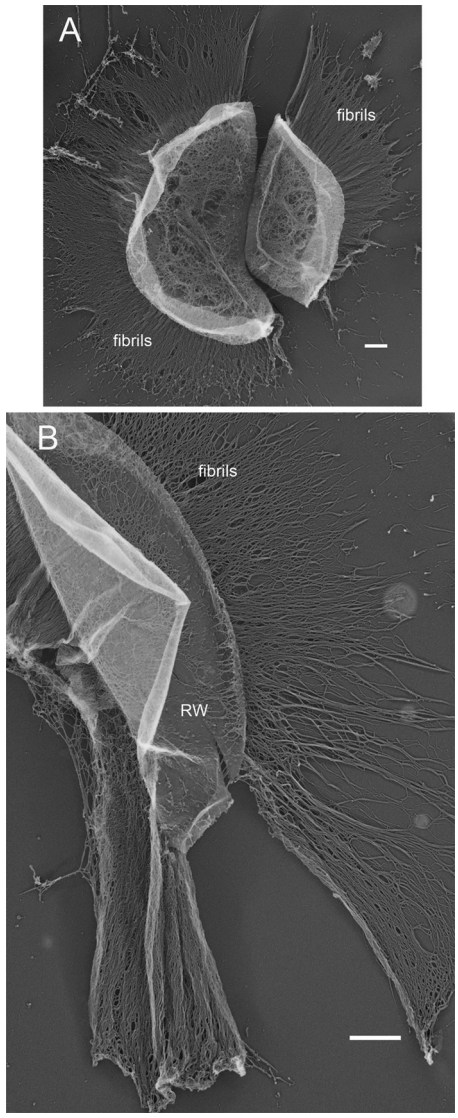

FIG 9 Shells adsorbed to glass and freeze-dried. (A) Two shells with associated fibrils. (B) Shell showing retaining wall and fibrils. Bars, 500 nm.

images of *n*-hexane extraction are included in File S7 in the supplemental material.

Features of the nonapical cell. (i) Lipid bodies. Figure 16A shows a cross-fracture through the nonapical portion of a cell and its contiguous h-ECM. Prominent in the cytoplasm is an organelle, designated a lipid body (L), that presumably corresponds to the Nile red-positive inclusions in Fig. 11C and D and 13 (see File S3 in the supplemental material). By Raman spectroscopy, these inclusions have been shown to contain botryococcenes (71), although this assay does not rule out the presence of additional components. In Fig. 16B and C, a *B. braunii* lipid body is shown to be similar in appearance to lipid bodies from a second trebouxiophyte, *Auxenochlorella protothecoides*, that produces triacylglycerol (TAG) (51), but not liquid hydrocarbons.

The *B. braunii* lipid bodies are invariably located in the cell interior, associated with both the ER/nuclear envelope and the chloroplast envelope, as is also the case for the chlorophyte *Chlamydomonas reinhardtii* (18). No images indicate that their contents are directly secreted into the extracellular matrix. Taken together, these observations suggest that the *B. braunii* lipid bodies may serve to store liquid botryococcenes, and possibly other products, for future mobilization.

TABLE 1 Glycosyl composition of isolated *B. braunii* shells

Glycosyl residue	Mass (μg)[a]	Mol%[a,b]
Arabinose (Ara)	83.5	46.7
3-Methyl-arabinose	7.3	3.7
Rhamnose (Rha)	ND[c]	
Fucose (Fuc)	ND	
Xylose (Xyl)	ND	
Glucuronic acid (GlcA)	ND	
Galacturonic acid (GalA)	ND	
Mannose (Man)	0.5	0.2
Galactose (Gal)	77.8	36.3
6-Methyl-galactose	7.6	3.3
Glucose (Glc)	0.9	0.4
N-Acetyl galactosamine (GalNAc)	ND	
N-Acetyl glucosamine (GlcNAc)	ND	
N-Acetyl mannosamine (ManNAc)	ND	
Deoxyhexoses[d]	18.3	9.3
Total carbohydrate	195.8	
Total protein[e]		1.25

[a] Two hundred micrograms of starting material was analyzed by GC-MS of alditol acetate-derivatized monosaccharides.
[b] Values are expressed as mole percent of total carbohydrate.
[c] ND, not detected by either the alditol acetate method shown or the TMS derivatization method (not shown).
[d] Two deoxyhexoses were detected by GC-MS analysis of the TMS method but did not match available standards and thus were not positively identified.
[e] Total protein was determined by Bradford assay and is reported as a percentage of the total weight of the sample.

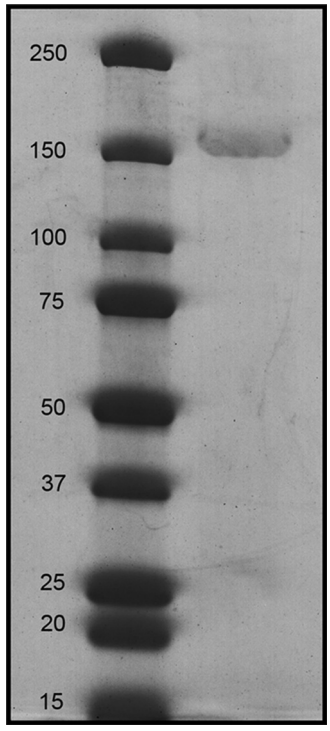

FIG 10 SDS-PAGE of shell preparation showing a single band comigrating with the 150-kDa marker.

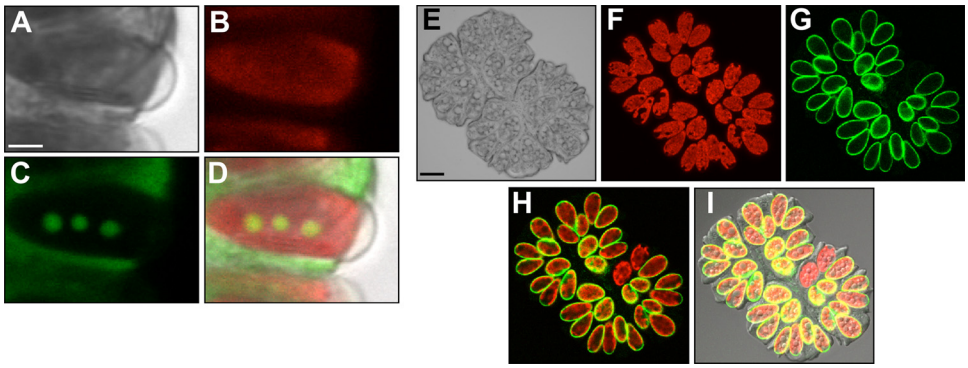

FIG 11 Nile red and Congo red staining of *B. braunii* colonies. All images were taken from a single *z* axis of the same colony. (A to D) Close-up images of the edge of a Nile red-stained colony. (A) DIC image of a Nile red-stained colony. Bar, 10 μm. (B) Chlorophyll autofluorescence channel. (C) Nile red channel, false colored green. (D) Merge of DIC, Nile red, and chlorophyll autofluorescence images. (E to I) Congo red-stained *B. braunii* colony. (E) DIC image of a single colony stained with Congo red. Bar, 10 μm. (F) Chlorophyll autofluorescence channel. (G) Congo red channel, false-colored green. (H) Merge of chlorophyll autofluorescence and Congo red images. (I) Merge of chlorophyll autofluorescence, Congo red, and DIC images. Note that two cells that appear to possess cell walls by DIC imaging are not stained by Congo red, suggesting a difference in cell wall chemical makeup or organization. The reason for this is unclear, but as it was a common observation it merits future investigation.

(ii) Fenestrated ER. The nonapical ER associates with internal lipid bodies and Golgi bodies (Fig. 16; see File S3 in the supplemental material). In addition, the system of cortical fenestrated ER, prominent beneath the apical cell wall (Fig. 3 and 4), where botryococcenes are not secreted, continues beneath the nonapical cell wall (Fig. 17), where botryococcenes are secreted. Images of secretion pores in the nonapical cell membrane are presented in File S4 in the supplemental material. As detailed in Discussion below, we propose that Golgi body-derived polysaccharide cell wall components pass through the fenestrae and pores in both apical and nonapical domains, while in nonapical regions, botryococcenes are also elaborated, in conjunction with the nonapical ER membrane, and are directly transferred into the cell membrane, after which they cross the cell wall and enter the h-ECM.

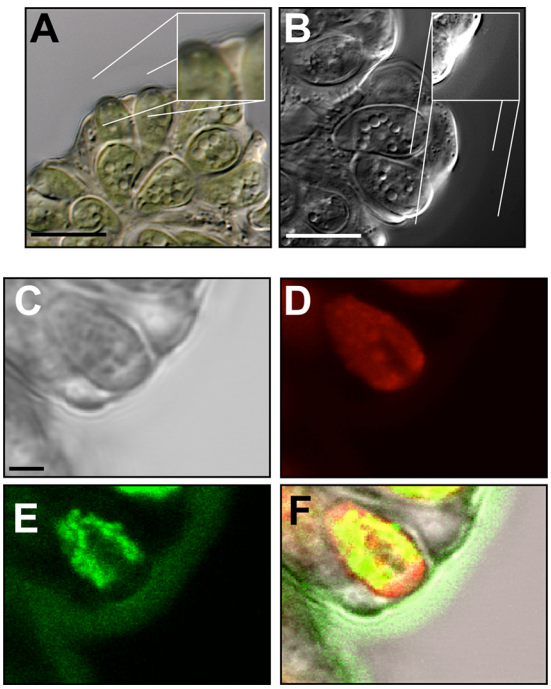

FIG 12 DIC imaging and mPAS staining of *B. braunii* colonies. All images were taken from a single *z* axis of the same colony. (A) Color DIC microscopy image of a colony with enlarged image of the colony edge. Bar, 10 μm. (B) Black-and-white DIC microscopy image of a colony with enlarged image of the colony edge showing presence of a colony sheath. Bar, 10 μm. (C to F) Close-up images of the edge of an mPAS-stained colony. (C) DIC image of an mPAS-stained colony. Bar, 2 μm. (D) Chlorophyll autofluorescence channel. (E) mPAS channel, false colored green. (F) Merge of DIC, mPAS, and chlorophyll autofluorescence images.

DISCUSSION

The combined application of TEM, histochemistry, and biochemical analysis utilized in this study provided a number of novel insights into the organization and composition of *B. braunii* race B colonies. Our findings pertaining to the ECM and its polysaccharide and hydrocarbon components are discussed below.

Retaining-wall morphology and functions. The retaining wall represents a unique and fascinating feature of *B. braunii* colonial organization.

The narrow nonfibrous retaining wall, which occasionally fractures into two sublayers, adopts 3 configurations. (i) When associated with a cell apex, it contacts the apical cell wall with its inner face. Its outer face is studded with "toothpaste tubules," a layer of granular material, and an extensive sheath of fibrils that are continuous with the tubules (Fig. 1 to 4) and presumably serve to interface between the colony and its aqueous and biological environment. (ii) When serving as an intercellular drape to sequester the hydrocarbon ECM, its outer face harbors the granules and fibrils but is devoid of tubules (Fig. 1, 2, and 5). We interpret this pattern as indicating that the tubules represent fibrillar material being secreted from the cell and, hence, absent when cell contact is lost. (iii) When serving as a "zipper" wall, the drape harbors the granules, at least initially, but is devoid of fibrils (Fig. 6).

Several candidate secretion pores have been found in the apical cell membrane (Fig. 4C; see File S3 in the supplemental material). Since images of secretion pores are rarely captured by electron microscopy, except in cases of massive exocytosis (21), these pores are apparently relatively long-lived. As developed below, we propose that polysaccharides pass through such pores and then either integrate into the cell wall in nonapical domains or else cross the

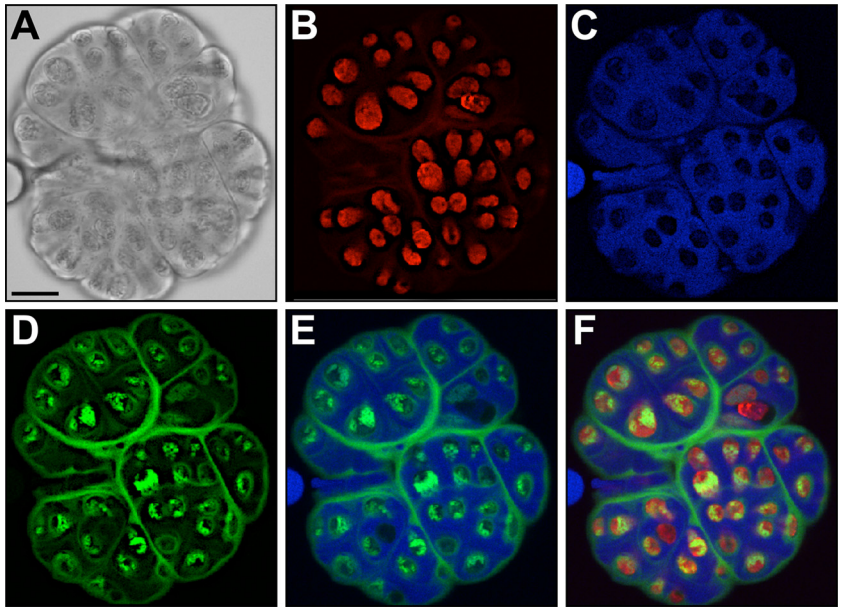

FIG 13 Nile red and mPAS costaining of a *B. braunii* colony. All images were taken from a single *z* axis of the same colony. (A) DIC image of a single *B. braunii* colony that was stained with Nile red and mPAS. Bar, 10 μm. (B) Chlorophyll autofluorescence channel. (C) Nile red channel, false colored blue. (D) mPAS channel, false colored green. (E) Merge of Nile red and mPAS images. (F) Merge of Nile red, mPAS, and chlorophyll autofluorescence images.

cell wall and integrate into the retaining wall and its associated sheath fibrils in apical domains.

The homogeneous granules of the retaining wall resemble proteins, an inference supported by biochemical analysis (see below). Since tubules enter the granular layer in a toothpaste configuration and exit in a fibrillar configuration, we posit that the granule proteins play a role in this conversion.

The presence of uniformly sized retaining-wall "shells" in the growth medium (Fig. 7 to 9) has been noticed in prior EM studies (5), where images have been interpreted to indicate that wall segments are severed and released from cell apexes, leaving behind cells that lack apical walls. We have not encountered such cells in our micrographs—all apical domains are covered by both cell and retaining walls—but cannot rule out a loss followed by the rapid synthesis of a replacement. An apical origin for the shells is suggested by their uniform size and curvature, but the alternative—that shells arise via excision of drape segments—has not been ruled out. Regardless of shell origin, there presumably exists a mechanism for splicing together the sites of shell excision so that an intact retaining wall is restored and h-ECM material is not lost.

TABLE 2 Glycosyl linkage analysis for carbohydrates in isolated *B. braunii* shells

Glycosyl linkage[a]	% Present[b]
Terminally linked[c] arabinofuranosyl (t-Araf)	11.9
2-Linked arabinofuranosyl (2-Araf)	19.7
4-Linked arabinopyranosyl or 5-linked arabinofuranosyl (4-Ara or 5-Araf)	0.1
Terminally linked deoxyhexose (t-deoxyhexose)[d]	6.1
2-Linked deoxyhexose (2-deoxyhexose)[d]	2.1
Terminally linked mannopyranosyl (t-Man)	0.5
3-Linked mannopyranosyl (3-Man)	0.2
Terminally linked galactofuranosyl (t-Galf)	2.1
Terminally linked galactopyranosyl (t-Gal)	1.1
3-Linked galactopyranosyl (3-Gal)	0.7
2-Linked galactopyranosyl (2-Gal)	0.9
4-Linked galactopyranosyl (4-Gal)	4.5
2,3-Linked galactopyranosyl (2,3-Gal)	31.7
2,4-Linked galactopyranosyl (2,4-Gal)	16.6
3,4,6-Linked galactopyranosyl (3,4,6-Gal)	1.8

[a] One thousand micrograms of starting material was analyzed by GC-MS of PMAA-derivatized monosaccharides.
[b] Values are expressed as percent of total carbohydrates found in the sample.
[c] Terminally linked refers to linkage at the C-1 position.
[d] Corresponding to unidentified deoxyhexoses in Table 1.

Retaining-wall and colony partitioning. When a colony expands in cell number and size and then gives rise to daughter colonies, each daughter must inherit an intact retaining wall or risk losing its h-ECM endowment. An obvious mechanism to accomplish this would be the involution of the retaining wall into the colony interior, followed by splicing events. Figure 13 shows that mPAS-positive material, continuous with the mPAS-positive layer surrounding the colonies, subdivides large colonies into smaller lobes, suggesting that the retaining wall indeed penetrates the colony interior.

Figure 6 shows a fortuitous cross-fracture that captures the mechanism for colony penetration—fortuitous in that such regions are presumably usually obscured by liquid hydrocarbons. A drape, no longer bearing fibrils, folds in on itself to form a structure resembling a zipper, with a central layer of granules flanked by two layers of retaining wall. The zipper extends into the h-ECM until it becomes masked by liquid hydrocarbon. Not yet known is whether the granules accompany deeper ingrowth or whether the interior version of the zipper becomes granule free and consists of two apposing retainer walls.

The ultrastructure of the zipper suggests a hypothesis to explain a key feature of *B. braunii* organization, namely, its ability to bud off daughter colonies from a mother colony without losing its hydrocarbon endowment, an excision process

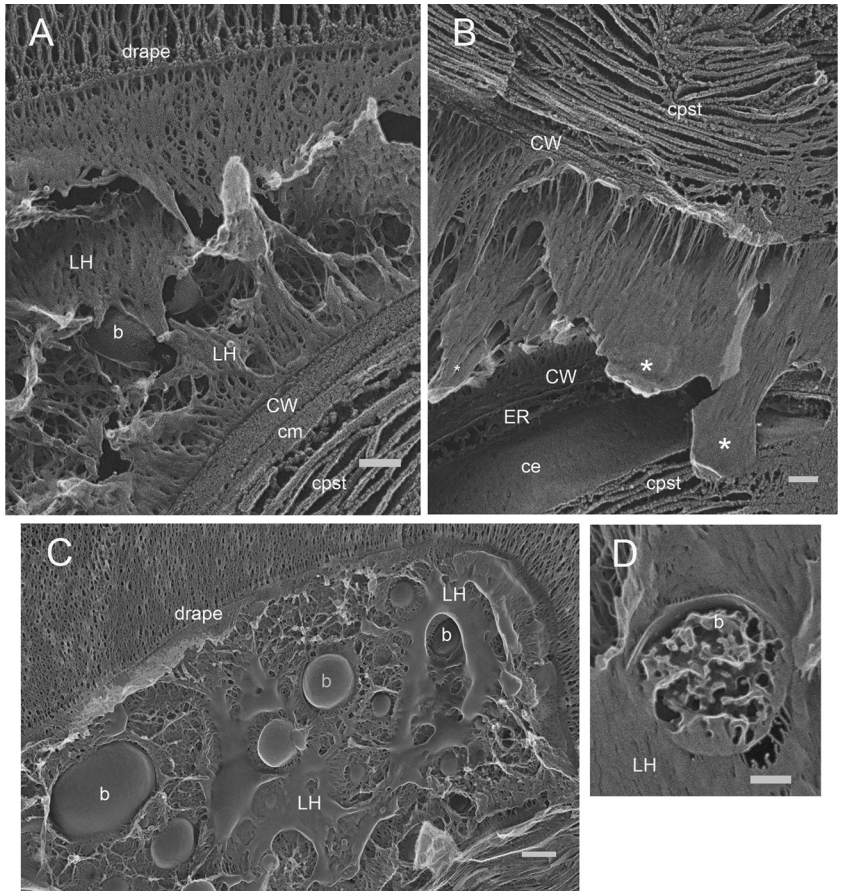

FIG 14 LH ECM. (A) LH relationship to internal cell wall and retaining-wall drape; b, balloon; cm, cell membrane; cpst, chloroplast. Bar, 100 nm. (B) Fracture-induced "splat" (asterisks) of LH over previously fractured cell; ce, chloroplast envelope; cpst, chloroplast. Bar, 100 nm. (C) LH in a rivulet configuration; b, balloon. Bar, 250 nm. (D) Cross-fractured balloon (b). Bar, 100 nm.

that is readily triggered by applying pressure to a coverslip overlying a colony. The central granular domain, or perhaps a domain of two apposing retainer walls if the granules fail to penetrate deeply, is posited to serve as a focus of slippage or shear, dissociating in response to natural or applied stimuli, thereby allowing the zipper to peel apart into half-zippers, each a single retaining wall, that segregate with daughter lobes. Such dissociation may be facilitated by cells that adopt an apical orientation with respect to the zipper and initiate fibril formation via "toothpaste" secretion. The fibrils would then serve to push the zipper, and hence the daughter colonies, apart.

Many questions are raised by this proposal. By what mechanism does the drape become fibril free at the drape-zipper junction? How are the timing and position of zipper ingrowth regulated and coordinated with cell division? Does a single zipper grow from one surface to the opposite side, or do two or more ingrowing zippers meet and fuse? What is the natural stimulus for initiating zipper dissociation? Do the granules, if present in the interior, play an active or passive role, and what is the relationship, if any, between the zipper mechanism and the accumulation of shells in the growth medium?

The fibrillar sheath. A *B. braunii* colony presents itself to its ecosystem as a dense ball of intertwined polysaccharide fibrils. An obvious function of this sheath, as with all algal ECMs, is to mediate an appropriate interface with the growth milieu; a second may be to aid in flotability; a third may be to protect from predators/pathogens.

It may also mediate symbiosis. While there are reports of axenic cultures of *B. braunii* (3, 23–26, 40, 60, 61, 64, 66, 68, 72, 78), maintaining the cultures as axenic over time has been difficult, raising the possibility of symbiotic relationships. The surface of the sheath frequently carries one or more associated bacteria (see Fig. S1-3 of File S1 in the supplemental material), whereas bacteria are never observed within the sheath interior. Possibly, symbiotic exchanges between *B. braunii* and fibril-recognizing bacteria occur at the sheath boundaries.

Retaining-wall chemistry. Oligosaccharides rich in arabinose and galactose are added to Ser, Thr, and Hyp residues of hydroxyproline-rich glycoproteins (HRGPs) in chlorophyte green algae (30); genomic evidence for HRGPs has also been obtained for prasinophyte (77), trebouxiophyte, and charophyte (J.-H. Lee, unpublished data) green algae. In contrast, free arabinose-galactose polysaccharides have to date been reported only in land plants (30) and mycobacteria (75).

Assays of isolated retaining walls/fibrillar sheaths (shells), which are 97.9% carbohydrate (Table 1), reveal that 80% of the sugars are unusual polymers of arabinose and galactose; third in abundance (~10%) are two unidentified deoxyhexoses. It is not

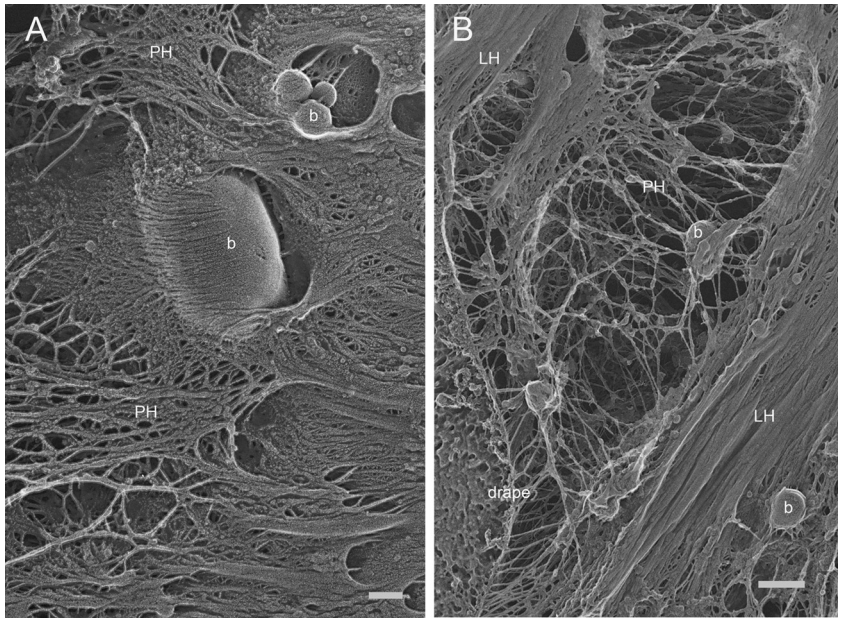

FIG 15 *n*-Hexane-extracted h-ECM. (A) Fully extracted region with polymerized hydrocarbons (PH) and balloons (b). Bar, 100 nm. (B) Partially extracted region with PH, persistent LH, and balloons (b). Bar, 250 nm.

known how these components are distributed between the fibrils and the retaining wall, but one hypothesis, concordant with their relative morphological abundance, is that arabinose and galactose form the fibrils and the deoxyhexoses, which are important ECM components in bacteria (33), form the retaining wall.

Shells also contain 1.25% protein. A single polypeptide migrating as a 150-kDa species is detected by SDS-PAGE of shell samples (Fig. 10), where some of its mass may be sugar if the protein is glycosylated. We propose that this polypeptide corresponds to the granules that appear to mediate the transformation of the toothpaste product into a fibrillar configuration and that persist in drapes, copurify with shells, and accompany retaining walls in their initial zipper configuration.

Cell wall morphology and chemistry. The retaining wall is narrow (~15 nm), with its etched inner face resembling concrete (Fig. 8C; see Fig. S7-1 to -3 of File S7 in the supplemental material). In contrast, the cell wall is much thicker (~50 nm), fractures into 2 layers, and is formed of fine filaments (Fig. 3A to C and 4A; see Fig. S3-1 and -2 of File S3 in the supplemental material). The cell wall has been proposed to be composed of polysaccharide (31), and its intense staining with Congo red (Fig. 11E to I) indicates it likely contains a β-1,4-glucan component, possibly but not necessarily cellulose, since Congo red can bind other β-1,4- and/or β-1,3-glucan polymers in addition to cellulose.

The secretory system. A *B. braunii* cell secretes three classes of ECM materials: (i) the polysaccharides of the cell wall and the retaining wall/fibrillar sheath, (ii) the presumed proteinaceous granules associated with the retaining wall, and (iii) the hydrocarbons of the h-ECM.

As noted in the introduction, botryococcenes are believed to be synthesized in association with the cytoplasmic face of the ER, and the enzyme activity associated with botryococcene biosynthesis is membrane associated (58). The bulk of the nonapical *B. braunii* ER takes the form of a cisternum contiguous to the cell membrane that apparently extends around the entire nonapical cell cortex (Fig. 17; see File S3 in the supplemental material), a configuration that is highly suited to secreting hydrocarbons to the cell exterior. We therefore propose that the hydrocarbons "melt into" the ER and then the plasma membrane, cross the cell wall, and are deposited into the h-ECM. The continuous "spikey" layer of liquid hydrocarbon directly contiguous to the cell wall (Fig. 14, 16, and 17) may represent newly secreted product.

The ECM polysaccharides, in contrast, are presumably synthesized by glycosyltransferases in the Golgi body, as previously suggested (58); packaged in vesicles; and delivered to the cell membrane for secretion. Were it the case that the cortical ER created a double-membrane barrier between the cytoplasm and the cell membrane, such a secretion mechanism would not be possible. Instead, the cortical ER is perforated by abundant fenestrae that expose the cell membrane to the cytoplasm (Fig. 3, 4, and 17). We propose that the fenestrae allow vesicle-mediated secretion. In this model, Golgi vesicles would dock at the fenestrae and deliver their contents to the exposed cell membrane, in the process creating the relatively long-lived secretion pores noted earlier. Golgi vesicles containing cell wall and retainer wall/sheath polysaccharides and granule proteins would, in this model, all utilize the fenestral ports. The presence of a highly developed Golgi body in the apical region and a more modest Golgi endowment in the cell interior suggests a more specific model: the apical Golgi body may provision the polysaccharides for the enormous project of producing the extensive retaining-wall–sheath–drape–zipper system, while the interior Golgi body delivers polysaccharide to the nonapical ER fenestrae for the more modest project of building the cell wall.

To our knowledge, the only other example of fenestrated ER is the annulate lamellar system, most commonly found in oocytes and in embryonic and neoplastic cells (27). Annulate lamellae occur in stacked arrays in association with a central nucleus, and their fenestrae are considered to be modified versions of nuclear

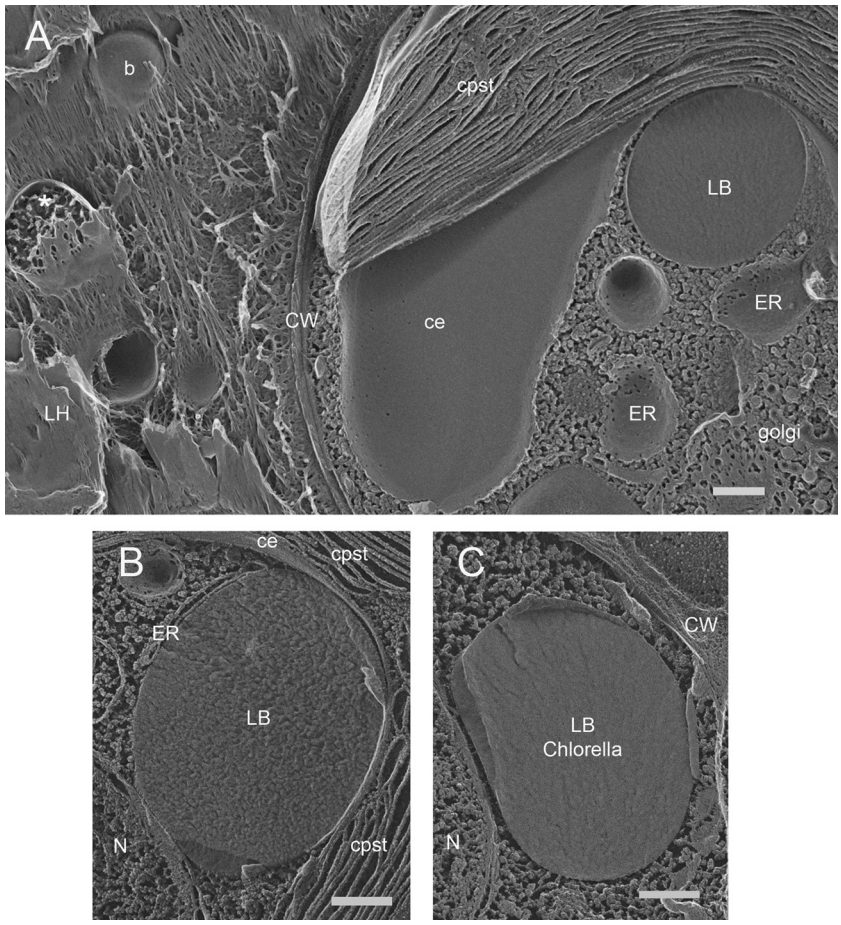

FIG 16 Lipid bodies. (A) Survey of nonapical cell interior and associated h-ECM. LB associates with the ER and chloroplast envelope (ce). cpst, chloroplast; b, balloon; asterisk, cross-fractured balloon. Bar, 250 nm. (B) Lipid body associated with ER/nuclear envelope around nucleus (N), ER element, and chloroplast envelope (ce). cpst, chloroplast. Bar, 250 nm. (C) Lipid body of *A. protothecoides* associated with nuclear envelope. N, nucleus. Bar, 200 nm.

pores. The cortical ER of *B. braunii* is clearly distinctive in both its nonstacked arrangement and cellular location, and the fenestrae are distinctive in morphology from *B. braunii* nuclear pores (see File S3 in the supplemental material). That said, structural elements are presumably necessary to create the fenestrae between apposed ER membrane sheets, and possibly a subset of nuclear-pore components has been recruited to this end.

The cortical ER does not engage in h-ECM secretion at the apical ends of the cells. One explanation might be that *B. braunii* possesses two physically independent ER systems: a nonapical ER

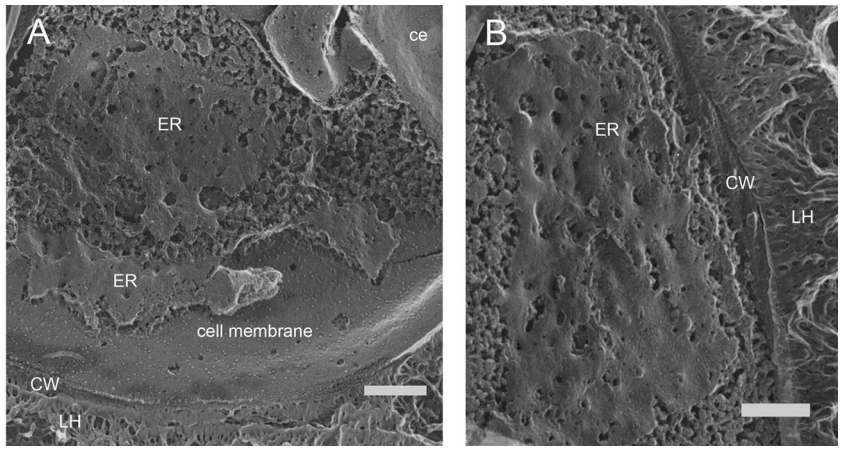

FIG 17 (A and B) Interior fenestrated ER in *en face* fracture. ce, chloroplast envelope. Bars, 250 nm.

endowed with h-ECM enzymes and an apical ER lacking these enzymes. However, the ER is believed to be a continuous system in all eukaryotic cells (14). The alternative, therefore, is that the *B. braunii* ER is a continuous system, with specific functions dictated by cellular location, which is consonant with many studies demonstrating that the ER can form locally differentiated domains (14). In *C. reinhardtii*, for example, one face of the ER can be seen to give rise to Golgi body-targeted vesicles, while the opposite face mediates lipid body formation (see Fig. 8C in reference 18).

ER profiles, often fenestrated, are also encountered in the cell interior, associated both with the *cis* face of the Golgi body (see File S3 in the supplemental material) and with lipid bodies. The lipid bodies are Nile red positive (Fig. 11 and 13) (71), and their EM morphology (Fig. 16A and B), including their enclosure in a membrane monolayer, is indistinguishable from that of the TAG-filled lipid bodies in other algae (Fig. 16C), where their close association with both chloroplast envelope and ER membranes is similar to the arrangement in *C. reinhardtii* (18). Raman spectroscopy indicates the presence of botryococcenes in these lipid bodies (71), and although the TAG levels in the B race have not been analyzed (44, 50), they are predicted to be low (<14%) compared to other algae (37).

We have not encountered images of lipid bodies in the cell periphery that appear poised for secretion into the h-ECM. Again making the assumption that the ER is a continuous system, one possibility is that some of the hydrocarbons synthesized in association with the cortical ER are routed, via lipid body-associated ER, to the lipid bodies for storage and future release.

The hydrocarbon extracellular matrix. Liquid botryococcenes fill the colony interior and coat the inner surfaces of drape walls and the outer surfaces of nonapical cell walls. Given that the material is deformable by the fracturing process (Fig. 14B), it is not possible to ascertain whether features of its organization, e.g., the delicate strands associated with the wall surfaces (Fig. 5 and 14B), are native or induced by sample preparation.

To distinguish between polymerized and liquid hydrocarbons, colonies were dried and treated with *n*-hexane, which selectively extracts the liquid phase (38). Abundant fibrillar material is revealed (Fig. 15), some in the form of narrow fibers and some as aggregates, where aggregation is possibly induced by the harsh drying and extraction procedures employed. Collectively, the images suggest that the polymerized fibers fill the ECM as a meshwork that provides mechanical stability to the colony, as has been previously proposed from the chemical analysis of these polymers (47). The meshwork may also create lacunae in the liquid-hydrocarbon phase to facilitate gas exchange in the colony interior.

The h-ECM also harbors round-to-oval inclusions that we designate balloons; similar structures are also evident in published thin-section studies (73), where they are interpreted as extracellular lipid bodies. The fact that the balloons persist after the liquid hydrocarbon is largely extracted by *n*-hexane indicates that they are stable entities and not simply morphological configurations of the liquid phase; the fact that they do not stain with Nile red (see Fig. S8-2 of File S8 in the supplemental material) indicates that they are not lipid bodies. When cross-fractured, they are found to contain aggregates of amorphous material (Fig. 14D and 16A).

We offer a proposal for the origin of balloons in the context of a peculiar feature of *B. braunii* colony organization. Should any cell in a colony die, as has been reported in late-stage cultures (11) and observed at earlier stages in our studies (T. L. Weiss and T. P. Devarenne, unpublished data), then the dead cell would by definition be trapped inside the colony by the retaining wall. Possibly *B. braunii* has evolved a senescence/apoptosis mechanism for dealing with this eventuality, with useful end products provisioning the living cells in the colony and nondegradable end products taking the form of balloons and the additional unidentified debris that litters the h-ECM. Evidence in support of this hypothesis may come from future genomic/transcriptomic identification of senescence/apoptosis-related genes in the *B. braunii* genome/expression profile.

Implications for biofuel applications. Our images indicate that *B. braunii* produces and secretes its high-value hydrocarbon products via a uniquely organized fenestrated ER system and that these products are sequestered within the colony via the specialized retaining wall. Ongoing efforts to identify the genes responsible for the biosynthesis of these products and to express them in fast-growing organisms may well be frustrated if there exist additional ER-localized and/or cell membrane-localized features (e.g., secretion mechanisms) that are required for execution of the pathway.

An alternative approach might be to characterize the structure of the retaining wall and identify inhibitors that prevent its formation and/or mechanical mechanisms to disrupt it, releasing single cells. Selection on these cells, under various light/growth conditions and with or without mutagenesis, would then be applied for such traits as unicellular viability, enhanced growth rates, and botryococcene secretion. Such single cells, if viable, could also be subjected to targeted genetic manipulation, a challenging project using an obligate colonial organism like *B. braunii*, where a sexual stage has not been identified. The understanding of *B. braunii* colonial organization provided in this report is expected to lend guidance to such approaches.

Evolutionary perspective. A colonial lifestyle has been adopted at numerous junctures in evolutionary history (59). *B. braunii* depends on its colonial organization to retain its hydrocarbon products for buoyancy, and hence access to light, and we document that a novel system, the retaining wall/sheath, mediates this trait. Biosynthesis of the retaining wall/sheath is a shared endeavor of all the cells in a colony and is presumably synchronized with rates of cell and hydrocarbon proliferation. The ingrowth of the retaining wall to generate daughter colonies is presumably also under some sort of coordination, as is the regular excision of retaining-wall segments (shells) during growth. Granted that unique solutions to the challenge of organizing multicellularity have repeatedly arisen, the bauplan evolved by the *Botryococcus* lineage is novel, elegant, and, judging by its ancient history and diversity, highly robust.

ACKNOWLEDGMENTS

This work was supported by contract DE-EE0003046 awarded to the National Alliance for Advanced Biofuels and Bioproducts (NAABB) from the U.S. Department of Energy. Carbohydrate MS analysis at the CCRC is supported in part by the Department of Energy-funded (DE-FG02-93ER-20097) Center for Plant and Microbial Complex Carbohydrates. The Olympus FV1000 confocal microscope acquisition at the Texas A&M University Microscopy and Imaging Center was supported by the Office of the Vice President for Research at Texas A&M University.

We thank Shayani Pieris and Richard Sayre for *Auxenochlorella protothecoides* samples and Michael Devarenne, Swamp-Side Studio, for production of the *B. braunii* colony model (Fig. 1).

ADDENDUM IN PROOF

After acceptance of this manuscript, we learned of an additional study on *B. braunii* ultrastructure (T. Noguchi and F. Kakami, J. Plant Res. 112:175-186, 1999) that documents the presence of a fenestrated ER beneath the cell membrane and associated with the Golgi apparatus. This study was done on the A race of *B. braunii*, indicating that this type of ER may be conserved among the three races of *B. braunii*.

REFERENCES

1. **Adam P, Schaeffer P, Albrecht P.** 2006. C_{40} monoaromatic lycopane derivatives as indicators of the contribution of the alga *Botryococcus braunii* race L to the organic matter of Messel oil shale (Eocene, Germany). Org. Geochem. **37**:584–596.
2. **Audino M, Grice K, Alexander R, Kagi RI.** 2002. Macrocyclic alkanes in crude oils from the algaenan of *Botryococcus braunii.* Org. Geochem. **33**: 979–984.
3. **Baba M, Ioki M, Nakajima N, Shiraiwa Y, Watanabe MM.** 2012. Transcriptome analysis of an oil-rich race A strain of *Botryococcus braunii* (BOT-88-2) by de novo assembly of pyrosequencing cDNA reads. Bioresour. Technol. **109**:282–286.
4. **Banerjee A, Sharma R, Chisti Y, Banerjee UC.** 2002. *Botryococcus braunii*: a renewable source of hydrocarbons and other chemicals. Crit. Rev. Biotechnol. **22**:245–279.
5. **Berkaloff C, et al.** 1984. Variability of cell-wall structure and hydrocarbon type in different strains of *Botryococcus braunii.* J. Phycol. **20**:377–389.
6. **Bertheas O, Metzger P, Largeau C.** 1999. A high molecular weight complex lipid, aliphatic polyaldehyde tetraterpenediol polyacetal from *Botryococcus braunii* (L race). Phytochemistry **50**:85–86.
7. **Blackburn KB.** 1936. A reinvestigation of the alga *Botryococcus braunii* Kützing. Trans. R. Soc. Edinburgh **58**:841–854.
8. **Brassell SC, Eglinton G, Mo FJ.** 1986. Biological marker compounds as indicator of the depositional history of the Maoming oil shale. Org. Geochem. **10**:927–941.
9. **Brown AC, Knights BA, Conway E.** 1969. Hydrocarbon content and its relationship to physiological state in the green alga *Botryococcus braunii.* Phytochemistry **8**:543–547.
10. **Cane RF.** 1977. Coorongite, balkashite and related substances: an annotated bibliography. Trans. R. Soc. S. Aust. **101**:153–154.
11. **Casadevall E, et al.** 1985. Studies on batch and continuous cultures of Botryococcus braunii: hydrocarbon production in relation to physiological state, cell ultrastructure, and phosphate nutrition. Biotechnol. Bioeng. **27**:286–295.
12. **Ciucanu I, Kerek F.** 1984. A simple and rapid method for the permethylation of carbohydrates. Carbohydr. Res. **131**:209–217.
13. **Darken MA.** 1962. Absorption and transport of fluorescent brighteners by microorganisms. Appl. Microbiol. **10**:387–393.
14. **English AR, Zurek N, Voeltz GK.** 2009. Peripheral ER structure and function. Curr. Opin. Cell Biol. **21**:596–602.
15. **Frenz J, Largeau C, Casadevall E, Kollerup F, Daugulis AJ.** 1989. Hydrocarbon recovery and biocompatibility of solvents for extraction from cultures of Botryococcus braunii. Biotechnol. Bioeng. **34**:755–762.
16. **Gelpi E, Oro J, Schneider HJ, Bennett EO.** 1968. Olefins of high molecular weight in two microscopic algae. Science **161**:700–702.
17. **Glikson M, Lindsay K, Saxby J.** 1989. *Botryococcus*—a planktonic green alga, the source of petroleum through the ages: transmission electron microscopical studies of oil shales and petroleum source rocks. Org. Geochem. **14**:595–608.
18. **Goodson C, Roth R, Wang ZT, Goodenough U.** 2011. Structural correlates of cytoplasmic and chloroplast lipid body synthesis in Chlamydomonas reinhardtii and stimulation of lipid body production with acetate boost. Eukaryot. Cell **10**:1592–1606.
19. **Grung M, Metzger P, Liaaen-Jensen S.** 1989. Primary and secondary carotenoids in two races of the green alga *Botryococcus braunii.* Biochem. Syst. Ecol. **17**:263–269.
20. **Heuser JE.** 2011. The origins and evolution of freeze-etch electron microscopy. J. Electron. Microsc. (Tokyo) **60**(Suppl. 1):S3–S29.
21. **Heuser JE, Reese TS.** 1981. Structural changes after transmitter release at the frog neuromuscular junction. J. Cell Biol. **88**:564–580.
22. **Hillen LW, Pollard G, Wake LV, White N.** 1982. Hydrocracking of the oils of Botryococcus braunii to transport fuels. Biotechnol. Bioeng. **24**: 193–205.
23. **Ioki M, et al.** 2012. Modes of hydrocarbon oil biosynthesis revealed by comparative gene expression analysis for race A and race B strains of *Botryococcus braunii.* Bioresour. Technol. **109**:271–276.
24. **Ioki M, Baba M, Nakajima N, Shiraiwa Y, Watanabe MM.** 2012. Transcriptome analysis of an oil-rich race B strain of *Botryococcus braunii* (BOT-22) by de novo assembly of pyrosequencing cDNA reads. Bioresour. Technol. **109**:292–296.
25. **Ioki M, Baba M, Nakajima N, Shiraiwa Y, Watanabe MM.** 2012. Transcriptome analysis of an oil-rich race B strain of *Botryococcus braunii* (BOT-70) by de novo assembly of 5′-end sequences of full-length cDNA clones. Bioresour. Technol. **109**:277–281.
26. **Ioki M, Ohkoshi M, Nakajima N, Nakahira-Yanaka Y, Watanabe MM.** 2012. Isolation of herbicide-resistant mutants of *Botryococcus braunii.* Bioresour. Technol. **109**:300–303.
27. **Kessel RG.** 1992. Annulate lamellae: a last frontier in cellular organelles. Int. Rev. Cytol. **133**:43–120.
28. **Kitazato H, Asaoka S, Iwamoto H.** 1989. Catalytic cracking of hydrocarbons from microalgae. Sekiyu Gakkaishi **32**:28–34.
29. **Knights BA, Brown AC, Conway E, Middleditch BS.** 1970. Hydrocarbons from the green form of the freshwater alga *Botryococcus braunii.* Phytochemistry **9**:1317–1324.
30. **Lamport DT, Kieliszewski MJ, Chen Y, Cannon MC.** 2011. Role of the extensin superfamily in primary cell wall architecture. Plant Physiol. **156**: 11–19.
31. **Largeau C, Casadevall E, Berkaloff C, Dhamelincourt P.** 1980. Sites of accumulation and composition of hydrocarbons in *Botryococcus braunii.* Phytochemistry **19**:1043–1051.
32. **Maeda H, Ishida N.** 1967. Specificity of binding of hexopyranosyl polysaccharides with fluorescent brightener. J. Biochem. **62**:276–278.
33. **Maki, M, Renkonen R.** 2004. Biosynthesis of 6-deoxyhexose glycans in bacteria. Glycobiology **14**:1R–15R.
34. **Mastalerz M, Hower JC.** 1996. Elemental composition and molecular structure of *Botryococcus* alginite in Westphalian cannel coals from Kentucky. Org. Geochem. **24**:301–308.
35. **Maxwell JR, Douglas AG, Eglinton G, McCormick A.** 1968. Botryococcenes—hydrocarbons of novel structure from the alga *Botryococcus braunii* Kutzing. Phytochemistry **7**:2157–2171.
36. **McKirdy DM, Cox RE, Volkman JK, Howell VJ.** 1986. Botryococcanes in a new class of Australian non-marine crude oils. Nature **320**:57–59.
37. **Metzger P, Allard B, Casadevall E, Berkaloff C, Coute A.** 1990. Structure and chemistry of a new chemical race of *Botryococcus braunii.* J. Phycol. **26**:258–266.
38. **Metzger P, Berkaloff C, Casadevall E, Coute A.** 1985. Alkadiene-producing and botryococcene-producing races of wild strains of *Botryococcus braunii.* Phytochemistry **24**:2305–2312.
39. **Metzger P, Casadevall E.** 1987. Lycopadiene, a tetraterpenoid hydrocarbon from new strains of the green alga *Botryococcus braunii.* Tetrahedron Lett. **28**:3931–3934.
40. **Metzger P, Casadevall E.** 1992. Ether lipids from *Botryococcus braunii* and their biosynthesis. Phytochemistry **31**:2341–2349.
41. **Metzger P, Casadevall E, CoutÉ A.** 1988. Botryococcene distribution in strains of the green alga *Botryococcus braunii.* Phytochemistry **27**:1383–1388.
42. **Metzger P, Casadevall E, Pouet MJ, Pouet Y.** 1985. Structures of some botryococcenes: branched hydrocarbons from the B-race of the green alga *Botryococcus braunii.* Phytochemistry **24**:2995–3002.
43. **Metzger P, David M, Casadevall E.** 1987. Biosynthesis of triterpenoid hydrocarbons in the B-race of the green alga *Botryococcus braunii.* Sites of production and nature of the methylating agent. Phytochemistry **26**: 129–134.
44. **Metzger P, Largeau C.** 1999. Chemicals of *Botryococcus braunii*, p 205–260. *In* Cohen Z (ed), Chemicals from microalgae. Taylor & Francis, London, United Kingdom.
45. **Metzger P, Largeau C.** 2005. *Botryococcus braunii*: a rich source for hydrocarbons and related ether lipids. Appl. Microbiol. Biotechnol. **66**:486–496.
46. **Metzger P, Pouet Y, Bischoff R, Casadevall E.** 1993. An aliphatic polyaldehyde from *Botryococcus braunii* (A race). Phytochemistry **32**:875–883.
47. **Metzger P, Rager MN, Fosse C.** 2008. Braunicetals: acetals from condensation of macrocyclic aldehydes and terpene diols in *Botryococcus braunii.* Phytochemistry **69**:2380–2386.

48. **Metzger P, Rager MN, Largeau C.** 2007. Polyacetals based on polymethylsqualene diols, precursors of algaenan in *Botryococcus braunii* race B. Org. Geochem. **38**:566–581.
49. **Metzger P, Templier J, Largeau C, Casadevall E.** 1986. An *n*-alkatriene and some *n*-alkadienes from the A race of the green alga *Botryococcus braunii.* Phytochemistry **25**:1869–1872.
50. **Metzger P, Villarreal-Rosales E, Casadevall E, CoutÉ A.** 1989. Hydrocarbons, aldehydes and triacylglycerols in some strains of the A race of the green alga *Botryococcus braunii.* Phytochemistry **28**:2349–2353.
51. **Miao X, Wu Q.** 2006. Biodiesel production from heterotrophic microalgal oil. Bioresour. Technol. **97**:841–846.
52. **Moldowan JM, Seifert WK.** 1980. First discovery of botryococcane in petroleum. J. Chem. Soc. Chem. Commun. **19**:912–914.
53. **Moreno N, Bougourd S, Haseloff J, Feijó JA.** 2006. Imaging plant cells, p 769–787. *In* Pawley JB (ed), Handbook of biological confocal microscopy, 3rd ed. Springer Science and Business Media, New York, NY.
54. **Niehaus TD, et al.** 2012. Functional identification of triterpene methyltransferases from *Botryococcus braunii* race B. J. Biol. Chem. **287**:8163–8173.
55. **Niehaus TD, et al.** 2011. Identification of unique mechanisms for triterpene biosynthesis in *Botryococcus braunii.* Proc. Natl. Acad. Sci. U. S. A. **108**:12260–12265.
56. **Noguchi T, Watanabe H.** 1999. Brefeldin A effects on the trans-Golgi network and Golgi bodies in *Botryococcus braunii* are not uniform during the cell cycle. Protoplasma **209**:193–206.
57. **Nonomura AM.** 1988. *Botryococcus braunii* var. *showa* (Chlorophyceae) from Berkeley, California, United States of America. Jpn. J. Phycol. **36**: 285–291.
58. **Okada S, Devarenne TP, Murakami M, Abe H, Chappell J.** 2004. Characterization of botryococcene synthase enzyme activity, a squalene synthase-like activity from the green microalga *Botryococcus braunii*, race B. Arch. Biochem. Biophys. **422**:110–118.
59. **Ratcliff WC, Denison RF, Borrello M, Travisano M.** 2012. Experimental evolution of multicellularity. Proc. Natl. Acad. Sci. U. S. A. **109**:1595–1600.
60. **Rivas MO, Vargas P, Riquelme CE.** 2010. Interactions of *Botryococcus braunii* cultures with bacterial biofilms. Microb. Ecol. **60**:628–635.
61. **Sato Y, Ito Y, Okada S, Murakami M, Abe H.** 2003. Biosynthesis of the triterpenoids, botryococcenes and tetramethylsqualene in the B race of *Botryococcus braunii* via the non-mevalonate pathway. Tetrahedron Lett. **44**:7035–7037.
62. **Stasiuk LD.** 1999. Confocal laser scanning fluorescence microscopy of *Botryococcus* alginite from boghead oil shale, Boltysk, Ukraine: selective preservation of various micro-algal components. Org. Geochem. **30**: 1021–1026.
63. **Summons RE, Metzger P, Largeau C, Murray AP, Hope JM.** 2002. Polymethylsqualanes from *Botryococcus braunii* in lacustrine sediments and crude oils. Org. Geochem. **33**:99–109.
64. **Tanoi T, Kawachi M, Watanabe MM.** 2011. Effects of carbon source on growth and morphology of *Botryococcus braunii.* J. Appl. Phycol. **23**: 25–33.
65. **Templier J, Largeau C, Casadevall E.** 1984. Hydrocarbon formation in the green-alga *Botryococcus braunii.* 4. Mechanism of non-isoprenoid hydrocarbon biosynthesis in *Botryococcus braunii.* Phytochemistry **23**:1017–1028.
66. **Templier J, Largeau C, Casadevall E.** 1987. Hydrocarbon formation in the green-alga *Botryococcus braunii.* 5. Effect of various inhibitors on biosynthesis of non-isoprenoid hydrocarbons in *Botryococcus braunii.* Phytochemistry **26**:377–383.
67. **Templier J, Largeau C, Casadevall E.** 1991. Biosynthesis of normal alkatrienes in *Botryococcus braunii.* Phytochemistry **30**:2209–2215.
68. **Templier J, Largeau C, Casadevall E.** 1993. Variations in external and internal lipids associated with inhibition of the resistant biopolymer from the A race of *Botryococcus braunii.* Phytochemistry **33**:1079–1086.
69. **Testa M, Gerbaudo S, Andri E.** 2001. *Botryococcus* colonies in Miocene sediments in the western Woodlark Basin, southwest pacific (ODP Leg 180). Proc. Ocean Drill. Prog. Sci. Results **180**:1–6.
70. **Traverse A.** 1955. Occurrence of the oil-forming alga Botryococcus in lignites and other Tertiary sediments. Micropaleontology **1**:343–348.
71. **Weiss TL, et al.** 2010. Raman spectroscopy analysis of botryococcene hydrocarbons from the green microalga Botryococcus braunii. J. Biol. Chem. **285**:32458–32466.
72. **Weiss TL, et al.** 2010. Phylogenetic placement, genome size, and GC-content of the liquid hydrocarbon producing green microalga *Botryococcus braunii* var. Berkeley (Showa) (Chlorophyta). J. Phycol. **46**:534–540.
73. **Wolf FR, Cox ER.** 1981. Ultrastructure of active and resting colonies of *Botryococcus braunii* (Chlorophyceae). J. Phycol. **17**:395–405.
74. **Wolf FR, Nemethy EK, Blanding JH, Bassham JA.** 1985. Biosynthesis of unusual acyclic isoprenoids in the alga *Botryococcus braunii.* Phytochemistry **24**:733–737.
75. **Wolucka BA.** 2008. Biosynthesis of D-arabinose in mycobacteria: a novel bacterial pathway with implications for antimycobacterial therapy. FEBS J. **275**:2691–2711.
76. **Wood PJ.** 1980. Specificity in the interaction of direct dyes with polysaccharides. Carbohydr. Res. **85**:271–287.
77. **Worden AZ, et al.** 2009. Green evolution and dynamic adaptations revealed by genomes of the marine picoeukaryotes Micromonas. Science **324**:268–272.
78. **Yonezawa N, Matsuura H, Shiho M, Kaya K, Watanabe MM.** 2012. Effects of soybean curd wastewater on the growth and hydrocarbon production of *Botryococcus braunii* strain BOT-22. Bioresour. Technol. **109**: 304–307.
79. **York WS, Darvill AG, McNeil M, Stevenson TT, Albersheim P.** 1986. Isolation and characterization of plant-cell walls and cell-wall components. Methods Enzymol. **118**:3–40.